JOURNAL OF PETROLOGY | VOLUME 40 | NUMBER 5 | PAGES 831–851 | 1999

Calculation of Peridotite Partial Melting from Thermodynamic Models of Minerals and Melts. III. Controls on Isobaric Melt Production and the Effect of Water on Melt Production

M. M. HIRSCHMANN[1,4]*, P. D. ASIMOW[2,4], M. S. GHIORSO[3] AND E. M. STOLPER[4]

[1]DEPARTMENT OF GEOLOGY AND GEOPHYSICS, UNIVERSITY OF MINNESOTA, 310 PILLSBURY DRIVE SE, MINNEAPOLIS, MN 55455-0219, USA

[2]LAMONT–DOHERTY EARTH OBSERVATORY, PALISADES, NY 10964, USA

[3]DEPARTMENT OF GEOLOGICAL SCIENCES, BOX 351310, UNIVERSITY OF WASHINGTON, SEATTLE, WA 98195, USA

[4]DIVISION OF GEOLOGICAL AND PLANETARY SCIENCES, 170-25 CALTECH, PASADENA, CA 91125, USA

RECEIVED APRIL 5, 1998; REVISED TYPESCRIPT ACCEPTED DECEMBER 2, 1998

We present a rigorous calculation of the isobaric entropy (S) change of the melting reaction for peridotite $(\partial S/\partial F)_P^{rxn}$, where F *is the melt fraction. Calculations at 1 and 2 GPa for fertile and depleted peridotite show that* $(\partial S/\partial F)_P^{rxn}$ *varies as a function of extent of melting, temperature, and residual mineral assemblage. Changes in reaction stoichiometry cause discontinuous changes in* $(\partial S/\partial F)_P^{rxn}$. *Although calculated* $(\partial S/\partial F)_P^{rxn}$ *varies by about a factor of two (from ~0·25 to ~0·5 J/K per g), such variations have relatively little effect on the formation of melt during adiabatic upwelling and a characteristic value suitable for peridotite partial melting at least up to 3 GPa is 0·3 J/K per g. Calculated variations in isobaric melt productivity,* $(\partial F/\partial T)_P$, *are large and have a significant effect on calculated adiabatic productivity,* $(\partial F/\partial P)_S$. *For partial melting of fertile peridotite, MELTS calculations suggest that near-solidus productivities are greatly reduced relative to productivities at higher melt fraction, owing to the incompatible behavior of* Na_2O *and the effect of this component on the liquidus temperature of partial melts. This behavior can also be demonstrated in simple model systems. Calculated near-solidus productivity for fractional or incremental batch melting of peridotite is lower than for batch melting, but after a small amount of melting (~2%), productivity for the fractional or incremental batch melting case is greater than that of batch melting. This too can be demonstrated both by MELTS calculations and by calculations in simple model systems. Productivities for systems enriched in incompatible components are systematically lower than those depleted in such components, though the total melt produced at any given temperature will be greater for an enriched system. Exhaustion of clinopyroxene from peridotite residua decreases calculated productivity by about a factor of four, and therefore extensive partial melting of harzburgitic residues is inhibited. Calculated isothermal addition of water to hot peridotite causes melting to increase roughly linearly with the abundance of water added to the system, in agreement with the trend recognized earlier for Mariana trough basalts. Melt production for calculated addition of a subduction fluid (45 wt % H_2O, 45% Na_2O, 10% K_2O) is only slightly greater than for pure water. If water addition to peridotite is not forced to be isothermal by an externally imposed heat sink or by buffering from low variance chemical reactions, then it will approach isenthalpic conditions, which will reduce melt production per increment of water added by about a factor of two. For heating of peridotite containing minor amounts of* H_2O, *calculations suggest that the extent of melting will remain small (<5%) until the temperature is sufficient to generate significant melt for an equivalent dry peridotite. Small degrees of melting deep*

*Corresponding author. Present address: Department of Geology and Geophysics, University of Minnesota, 310 Pillsbury Drive SE, Minneapolis, MN 55455-0219, USA. Telephone: 612-625-6689. Fax: 612-625-3819. e-mail: Marc.M.Hirschmann-1@umn.edu

in mantle source regions caused by alkalis, CO_2, and H_2O probably result in several distinct melting regimes where melt productivities are very small and melt compositions are strongly influenced by high concentrations of alkalis and/or volatiles. Such regions are almost certainly in the garnet peridotite stability field, and owing to the small extents of melting and low productivities in these deep melting zones, they are likely regions for development of extreme U-series disequilibria.

KEY WORDS: *mantle melting*; *peridotite*; *hydrous melting*; *ridges*; *arcs*

INTRODUCTION

Partial melting of the mantle is one of the chief mechanisms of energy and mass transfer between the Earth's interior and the surface, and has been a topic of intensive study for decades. As a result, there are now reasonable constraints on many aspects of mantle melting processes, including the volumes of melt formed in various tectonic environments, the temperatures and pressures prevailing during melting, and the compositions of mantle source regions. However, the energetics of mantle melting are only roughly understood and the quantitative effects of volatile components are yet to be described adequately.

Although understanding of mantle melting must be grounded in high-quality phase equilibria experiments, such experiments are not well suited for understanding the energetics of mantle melting or the effect of fluxing components such as H_2O on melt production. As is the case for understanding the relationship between source composition, melting process, and the composition of mantle melts (Hirschmann *et al.*, 1999), forward models linking phase equilibria to mass and energy balance are required. Here we apply the MELTS algorithm (Ghiorso & Sack, 1995) to the problem of isobaric melt production in the shallow mantle. MELTS has particular potential to aid understanding of melting behavior because it explicitly incorporates a quantitative description of melting energetics. Such energetics play key roles in natural processes yet cannot be inferred directly from experiments on complex systems.

In a companion paper (Hirschmann *et al.*, 1998*b*), we show that MELTS calculations capture the essential features of the phase equilibria of partially melting peridotite up to the lowest pressures of the garnet stability field. Although the calculations have inaccuracies, the extent of agreement with melting experiments on peridotitic compositions is sufficient to allow numerical simulations of mantle melting processes that lead to useful insights that are not otherwise available. In our earlier paper (Hirschmann *et al.*, 1998*b*), we described calculation methods for applying MELTS to peridotite partial melting problems, compared MELTS calculations with peridotite partial melting experiments (especially at pressures near 1 GPa), and reviewed the strengths and limitations of applications of the current MELTS calibration to peridotite partial melting calculations. In this paper, we use MELTS to address the influence of key variables affecting melt production in peridotitic source regions: the distribution of entropy among liquid and solid phases during melting and the amount of melt produced as a function of changing temperature at constant pressure (the 'isobaric productivity'), emphasizing in particular the effects of incompatible components (e.g. H_2O, K_2O, CO_2, etc.) on melt production at low melt fractions, and the amount of melt produced owing to fluxing of peridotite by H_2O-rich fluids.

For melting in response to adiabatic upwelling, a critical variable is the productivity, the amount of melt (F) generated per increment of upwelling. Productivity affects the total volume of melt (and hence the thickness of crust) generated from ascending mantle with a given entropy (or potential temperature; McKenzie, 1984). Also, variations in productivity influence the average depth of melting inferred from basalt geochemistry (Plank *et al.*, 1995) and may exert important controls on melt segregation processes (Spiegelman, 1993; Asimow *et al.*, 1995). In many treatments of adiabatic upwelling, the productivity is assumed to be constant (Klein & Langmuir, 1987; Niu & Batiza, 1991; Kinzler & Grove, 1992; Kinzler, 1997), but considerable uncertainty remains about the appropriate value to use and recent theoretical work (Asimow *et al.*, 1997) has shown that it probably increases significantly as melting proceeds (until exhaustion of cpx from the residue). Two variables that must be known in order to calculate adiabatic melt productivity are the isobaric change in entropy (S) associated with the melting reaction, $(\partial S/\partial F)_P^{rxn}$ (Asimow, 1997), and the isobaric melt productivity, $(\partial F/\partial T)_P$, where F is the mass fraction of melt relative to the original starting mass of peridotite. Neither of these variables is well characterized for peridotite–melt systems. Evaluation of these variables and what controls them is one focus of this paper.

Present understanding of the isobaric entropy of the melting reaction, $(\partial S/\partial F)_P^{rxn}$, is particularly problematic. Not only are the values of this variable poorly known, but just what it actually corresponds to and how it can be related to measurable quantities is not widely understood. Based on analogy with one-component systems, $(\partial S/\partial F)_P^{rxn}$ is commonly equated with the entropy of fusion (ΔS^{fus}) (McKenzie & Bickle, 1988; Scott, 1992; Iwamori *et al.*, 1995). This is a poor analogy for multicomponent systems, for which the 'entropy of fusion' is poorly defined. In one-component systems isobaric melting takes place at a fixed temperature and involves

conversion of a solid to a liquid of the same composition, and the entropy of fusion is just the difference in entropy between the coexisting, constant composition solid and liquid at this temperature and pressure. In contrast, isobaric melting of natural peridotite takes place over a range of temperatures, and the liquid formed does not have the same composition as the solid residue. Thus, for peridotite–melt systems, $(\partial S/\partial F)_P^{rxn}$ is affected by differences in liquid and solid composition and by variations in reaction stoichiometry as melting proceeds. Therefore, evaluation of this term in an expression for productivity requires detailed information about the specific entropies of solid and liquid phases as well as about reaction stoichiometry, and simple notions of the 'entropy of fusion' based on analogy with a one-component system (e.g. the difference in specific entropy between the bulk solid peridotite and a liquid of the same composition; or the difference in specific entropy between coexisting solids and liquids) are not applicable. MELTS is well suited to calculation of $(\partial S/\partial F)_P^{rxn}$ during partial melting of natural peridotite.

Knowledge of the isobaric productivity, $(\partial F/\partial T)_P$, of peridotite is also incomplete and experimental studies have yielded conflicting information. Some experimental studies suggest that productivity in peridotite systems is nearly constant from near the solidus to the exhaustion of cpx (Baker & Stolper, 1994; Robinson *et al.*, 1998), but others suggest that melting is eutectic-like in that significant melt is generated over a small temperature interval above the solidus (Jaques & Green, 1980), and still other studies suggest that $(\partial F/\partial T)_P$ is significantly smaller near the solidus than at higher melt fractions (Mysen & Kushiro, 1977; Walter & Presnall, 1994). The divergence of experimental evidence on this matter illustrates the difficulty of carrying out experiments near the solidus and underscores that the causes of variations in $(\partial F/\partial T)_P$, which propagate into adiabatic productivity, remain poorly understood. MELTS calculations can be used to gain a fuller understanding of the expected behavior of $(\partial F/\partial T)_P$ as melting proceeds and of expected variations related to melt removal or phase exhaustion.

Another topic of current interest is the effect of incompatible components present at higher than trace levels (e.g. Na_2O, K_2O, H_2O, CO_2) on peridotite melting. For example, melting in the mantle wedge above subduction zones is driven by addition of water-rich fluids or melts from the subducting slab (e.g. Gill, 1981; Tatsumi, 1983; Tatsumi *et al.*, 1986; Kushiro, 1987; Plank & Langmuir, 1988; Davies & Stevenson, 1992; Stolper & Newman, 1994). From studies of back-arc basin basalts from the Mariana trough, Stolper & Newman (1994) inferred that the water-rich component that fluxes the mantle wedge is rich in Na_2O and K_2O. By comparing the budgets of trace elements and water in these magmas, they inferred that the extent of melting experienced by peridotite in the mantle wedge depends approximately linearly on the amount of the slab-derived fluid and/or melt added to the peridotite. Melting experiments performed on peridotite with small amounts of added water (Hirose & Kawamoto, 1995) are consistent with the relationship inferred by Stolper & Newman up to the exhaustion of cpx. However, there have so far been no phase equilibrium calculations presented that explore this behavior or that describe the energetic consequences of addition of incompatible elements (of which water is a very important example) to partially molten peridotite. MELTS incorporates the effects of Na_2O, K_2O, and water on the thermodynamics of partially molten silicate systems, and therefore allows evaluation of the effects of such components on peridotite melting in the upper mantle.

THE ENERGETICS OF PERIDOTITE PARTIAL MELTING

If melting during mantle upwelling is adiabatic and reversible, then it is an isentropic process and the melt production for batch melting processes is given by

$$-\left(\frac{\partial F}{\partial P}\right)_S = \frac{\dfrac{C_p^{sol}+F(C_p^{liq}-C_p^{sol})}{T}\left(\dfrac{\partial T}{\partial P}\right)_F - \left(V^{sol}\alpha^{sol}+F(V^{liq}\alpha^{liq}-V^{sol}\alpha^{sol})+\left(\dfrac{\partial S_X}{\partial P}\right)_F\right)}{\dfrac{C_p^{sol}+F(C_p^{liq}-C_p^{sol})}{T\left(\dfrac{\partial F}{\partial T}\right)_P}+\left(\dfrac{\partial S}{\partial F}\right)_P^{rxn}} \quad (1)$$

(Asimow *et al.*, 1997). In this equation, C_p, V, and α are heat capacity, molar volume, and thermal expansivity. $(\partial T/\partial P)_F$ is the slope of a constant melt fraction isopleth and $(\partial F/\partial T)_P$ is the isobaric productivity (discussed in greater detail below); both of these derivatives can be estimated from detailed phase equilibrium measurements or from accurate thermodynamic calculations. $(\partial S/\partial F)_P^{rxn}$, the isobaric entropy of melt reaction, is given by

$$\left(\frac{\partial S}{\partial F}\right)_P^{rxn} = S_l - S_s + \left(\frac{\partial S_X}{\partial F}\right)_P \quad (2)$$

(Asimow *et al.*, 1997), where S_l is the specific entropy of the liquid, S_s the specific entropy of the bulk solid coexisting with that liquid, and $(\partial S_X/\partial F)_P$ is shorthand for the summation in equation (3), which accounts for the

changes in the entropy of the system as a result of redistribution of components between phases:

$$\left(\frac{\partial S_X}{\partial F}\right)_P = \sum_{i=1}^{n^l}\left(\left(\frac{\partial S^l}{\partial m_i^l}\right)_{T,P,m_{j\neq i}^l}\left(\frac{\partial m_i^l}{\partial F}\right)_{P,m_{j\neq i}^l}\right) + \sum_{i=1}^{n^s}\left(\left(\frac{\partial S^S}{\partial m_i^S}\right)_{T,P,m_{j\neq i}^s}\left(\frac{\partial m_i^S}{\partial F}\right)_{P,m_{j\neq i}^s}\right). \quad (3)$$

Here

$$\left(\frac{\partial S^{l\text{ or }s}}{\partial m_i^l}\right)_{T,P,m_{j\neq i}^{l\text{ or }s}}$$

is partial specific entropy of liquid or solid component i,

$$\left(\frac{\partial m_i^{l\text{ or }s}}{\partial F}\right)_{P,m_{j\neq i}^{l\text{ or }s}}$$

is the extensive change in mass of each liquid or solid component $m_i^{l\text{ or }s}$ as melting proceeds (i.e. the extensive equivalent of the stoichiometric reaction coefficient) and n^s is the sum of components in all the solid phases. It should be noted that in a one-component system, $(\partial S/\partial F)_P^{rxn}$ reduces to $S_l - S_s$, which is just the entropy of fusion. The term $(\partial S_X/\partial P)_F$ in the numerator of equation (1) represents the change in entropy owing to mineral reactions other than melting that occur when pressure changes. It is defined in the same way as $(\partial S_X/\partial F)_P$ in equation (3), except that P is a variable and F is held constant. This term can be important when mineral reactions, such as those associated with the garnet peridotite to spinel peridotite or spinel peridotite to plagioclase peridotite, occur (Asimow *et al.*, 1995), but otherwise is of less importance than the other terms in equation (1).

Calculation of $(\partial S/\partial F)_P^{rxn}$ requires (1) an inventory of the specific entropy of each component in each phase and (2) detailed knowledge of the proportions and compositions of coexisting phases as a function of melt fraction. At this time, MELTS is the only available model for calculating formally and rigorously (subject to its assumed thermochemical models of the various phases involved) the compositions and specific entropies of all phases along a path through the peridotite melting interval. Also, unlike other available models, MELTS incorporates estimates of the entropies of mixing of all phases. Although subject to uncertainties, MELTS thus allows us to explore the magnitude and variations of this term affecting adiabatic melting.

Using MELTS and equations (2) and (3), we have calculated $(\partial S/\partial F)_P^{rxn}$ for the fertile MM3 peridotite (Baker & Stolper, 1994) at 1 GPa from the solidus to the liquidus (Fig. 1). Except near the solidus, where $(\partial S/\partial F)_P^{rxn}$ approaches 0·5 J/K per g, calculated values of $(\partial S/\partial F)_P^{rxn}$ are <0·4 J/K per g, and between 3% and 50% melting they are in the narrow range of 0·3 ± 0·05 J/K per g. In detail, from the solidus to the liquidus, there are three distinct intervals in which $(\partial S/\partial F)_P^{rxn}$ (heavy solid curve) varies continuously. These regions of continuous variations are separated by discontinuities corresponding to the exhaustion of cpx and opx from the residue, so values of $(\partial S/\partial F)_P^{rxn}$ are distinct for systems with lherzolitic, harzburgitic, and dunitic residues. Such changes in $(\partial S/\partial F)_P^{rxn}$ owing to changes in the mineralogy of the residue are related to discontinuous changes in reaction stoichiometry [i.e. to changes in $(\partial S_X/\partial F)_P$; equation (3)]. Of the three regions, $(\partial S/\partial F)_P^{rxn}$ is lowest for harzburgitic residues and higher for dunitic and lherzolitic residues. Gradual increases in $(\partial S/\partial F)_P^{rxn}$ in the harzburgite and dunite regions reflect primarily rising temperature, as the higher heat capacity in silicate liquid relative to coexisting minerals results in the specific entropy of liquid increasing relative to solids with rising temperature. Significant variations in $(\partial S/\partial F)_P^{rxn}$ are predicted in the near-solidus lherzolitic region.

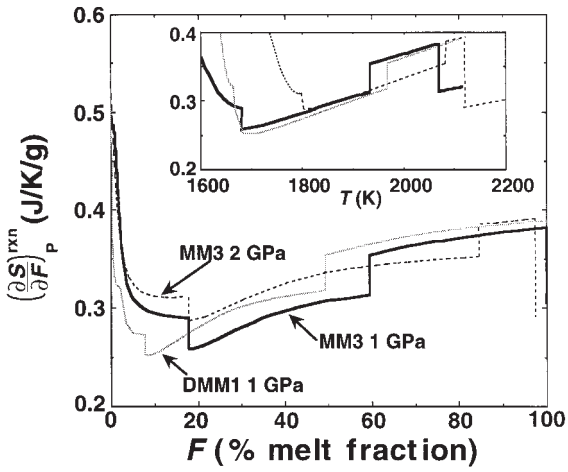

Fig. 1. MELTS calculation of $(\partial S/\partial F)_P^{rxn}$ as a function of melt fraction for the fertile MM3 peridotite composition at 1 GPa and 2 GPa and for the depleted DMM1 peridotite composition at 1 GPa. The trend for each calculation has three distinct regions, separated by discontinuous changes in $(\partial S/\partial F)_P^{rxn}$ that correspond to changes in the residual mineral assemblage. Below ~18% melting for MM3 (7% for DMM1), the residual assemblage is lherzolitic (ol + opx + cpx + sp). Above this melt fraction, the assemblage is harzburgitic (ol + opx ± sp). At higher melt fraction (~50% for DMM1, ~60 and ~80% for MM3 at 1 and 2 GPa), opx is eliminated from the residual assemblage and the residual assemblage is dunitic (ol ± sp). The sharp drops at >95% melting for MM3 correspond to the exhaustion of olivine in the residue (leaving only spinel). In the inset, the same data are plotted against temperature. This plot shows that when the residual assemblage is harzburgitic or dunitic, but not lherzolitic, $(\partial S/\partial F)_P^{rxn}$ depends mainly on temperature. In the lherzolitic region, $(\partial S/\partial F)_P^{rxn}$ is more strongly influenced by melt fraction. Regions at very high temperature that have low values of $(\partial S/\partial F)_P^{rxn}$ correspond to calculated stability of a tiny amount of chromite near the liquidus.

In Fig. 1, we compare the trend calculated for MM3 at 1 GPa with that calculated at 2 GPa and with that calculated for depleted DMM1 peridotite (Wasylenki *et al.*, 1996; Hirschmann *et al.*, 1998*b*) at 1 GPa. The trend of $(\partial S/\partial F)_P^{rxn}$ as a function of melt fraction is similar for all three calculations. In all cases, there are distinct regions corresponding to the different residual mineral assemblages, with the lowest values occurring for harzburgite assemblages, and highest values occurring near the solidus. Differences in absolute value reflect primarily the different temperature–melt fraction trajectories for the different cases. Thus, if the three calculations are compared as a function of temperature (see inset to Fig. 1), they differ little in the harzburgite and dunite regions for the different compositions when these overlap in temperature. In contrast, variations in $(\partial S/\partial F)_P^{rxn}$ in the lherzolite region are variable among the three compositions; these variations are related primarily to changes in melt composition and not to temperature, as large changes in $(\partial S/\partial F)_P^{rxn}$ are predicted in the near-solidus region over small temperature intervals.

The large calculated changes in $(\partial S/\partial F)_P^{rxn}$ in the lherzolite region are related primarily to variations in the Na_2SiO_3 component in the melt in this region (Hirschmann *et al.*, 1998*b*). The partial specific entropy of Na_2SiO_3 liquid,

$$\left(\frac{\partial S^{l}}{\partial m^{l}_{Na_2SiO_3}}\right)_{P,T,m^{l}_{i\neq Na_2SiO_3}} \text{ in equation (3)}$$

is 3·2 J/K per g at 1400°C and 1 GPa. This is significantly higher than that of other components calculated in the MELTS model, which are all between 2·6 and 2·7 J/K per g at 1400°C and 1 GPa, except for Fe_2SiO_4 (1·9 J/K per g) and Mg_2SiO_4 (2·85 J/K per g), so the increase in the concentration of Na_2O as the solidus is approached translates directly into an increase in $(\partial S/\partial F)_P^{rxn}$. It should be noted that because MELTS calculations exaggerate the concentration of Na_2O in near-solidus liquids (Hirschmann *et al.*, 1998*b*), the large calculated increases in $(\partial S/\partial F)_P^{rxn}$ near the solidus shown in Fig. 1 are also probably exaggerated.

Although calculated variations in $(\partial S/\partial F)_P^{rxn}$ through the melting interval of peridotite are rather large, equation (1) shows that adiabatic productivity is influenced by many variables. Therefore large variations in $(\partial S/\partial F)_P^{rxn}$ do not necessarily result in large variations in adiabatic productivity. Inspection of equation (1) shows that it is not the absolute magnitude of changes in $(\partial S/\partial F)_P^{rxn}$ that determines how $(\partial F/\partial P)_S$ varies, but the magnitude of those changes relative to other terms in the denominator. One way to gauge the impact of variations in $(\partial S/\partial F)_P^{rxn}$ on $(\partial F/\partial P)_S$ is to compare values of $(\partial F/\partial P)_S$ calculated rigorously by MELTS [i.e. allowing all variables in the right-hand side of equation (1) to vary continuously with F] with values calculated in the same way except with $(\partial S/\partial F)_P^{rxn}$ held at some arbitrary constant value. Values of $(\partial S/\partial F)_P^{rxn}$ (or actually of its less-rigorous equivalent 'ΔS^{fus}') used in the literature range from 0·25 J/K per g (McKenzie & Bickle, 1988; Scott, 1992) to 0·4 J/K per g (McKenzie & O'Nions, 1991). Recently, Kojitani & Akaogi (1997) estimated $(\partial S/\partial F)_P^{rxn} \approx 0{\cdot}40 \pm 0{\cdot}03$ J/K per g for peridotite partial melting from combined 1 atm calorimetric determinations of melting in a simple CMAS analogue system and estimated corrections for the effect of more complex compositions, pressure, and reaction stoichiometry. In Fig. 2, we compare the instantaneous adiabatic productivity calculated by MELTS [i.e. with variable $(\partial S/\partial F)_P^{rxn}$] with that calculated with $(\partial S/\partial F)_P^{rxn}$ set to constant values of 0·25, 0·30 and 0·40 J/K per g for the case of adiabatic batch melting of MM3 peridotite at 1 GPa at temperatures ranging from the solidus to the liquidus. The calculated productivity shown in Fig. 2 at any given melt fraction thus corresponds to the instantaneous productivity that would be applicable for batch melting along an adiabatic path that has that melt fraction at 1 GPa. As is evident from Fig. 2, adiabatic productivity calculated with $(\partial S/\partial F)_P^{rxn}$ set to 0·30 J/K per g is most similar to that calculated with variable $(\partial S/\partial F)_P^{rxn}$. Near the solidus, where $(\partial S/\partial F)_P^{rxn}$ varies most, adiabatic productivity is more sensitive to the larger variations in $(\partial F/\partial T)_P$ [also in the denominator in equation (1)] that are also occurring [see below and Asimow *et al.* (1997)], so $(\partial S/\partial F)_P^{rxn}$ variations have relatively little effect. The correspondence of the full MELTS calculation to the $(\partial S/\partial F)_P^{rxn} = 0{\cdot}30$ J/K per g approximation is particularly good for adiabats that at 1 GPa are between the solidus and the exhaustion of orthopyroxene at ~60% melting. Other constant values for $(\partial S/\partial F)_P^{rxn}$ reproduce the variable $(\partial S/\partial F)_P^{rxn}$ trend in productivity less accurately, although they do not affect the overall shape of the productivity function.

Our calculations show that the MELTS-predicted deviations from constant values of $(\partial S/\partial F)_P^{rxn}$ depicted in Fig. 1 have relatively little effect on the calculated adiabatic productivity at 1 GPa. Although not shown, values near 0·30 J/K per g also reproduce calculated $(\partial F/\partial P)_S$ trends for pressures at least up to 3 GPa and for other peridotite compositions, particularly between the solidus and exhaustion of cpx. We conclude that for most situations, 0·30 J/K per g is an appropriate constant value for calculation of adiabatic melting of peridotite in the shallow mantle up to the point of opx exhaustion. $(\partial S/\partial F)_P^{rxn}$ also appears in the expression for productivity during incrementally isentropic fractional fusion; the values quoted here for batch melting reactions are also likely to be appropriate for fractional fusion because the effect of the Na_2SiO_3 component will again be most pronounced near the solidus, where variations in $(\partial S/\partial F)_P^{rxn}$ are least

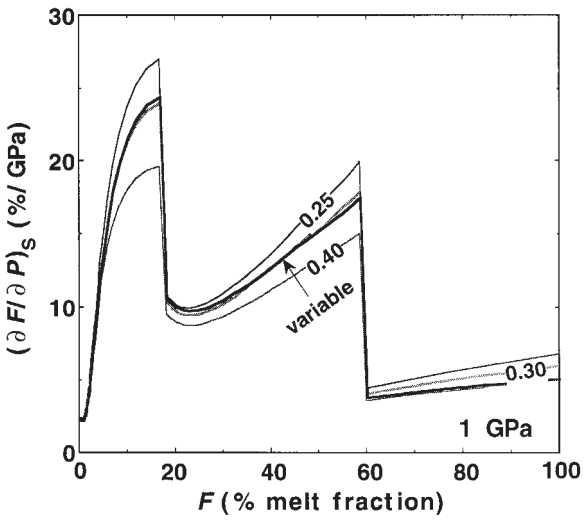

Fig. 2. Calculated adiabatic productivity, $(\partial F/\partial P)_S$ (in units of percent melting per GPa) plotted against extent of melting (in percent) at 1 GPa for the fertile MM3 peridotite composition. Higher extents of melting correspond to adiabats with higher potential temperatures (and entropies), which therefore have achieved higher extents of melting when they traverse the depth at which the pressure is 1 GPa. Calculations for the curve marked 'variable' are performed for the MM3 composition with values of all parameters on the right-hand side of equation (1) calculated with MELTS. Curves marked with numbers are calculated in the same manner, except that the value used for $(\partial S/\partial F)_P^{rxn}$ is held at a constant value (0·25, 0·3, and 0·4 J/K per g), rather than the value calculated with MELTS. The similarity between the 'variable' line and that calculated with $(\partial S/\partial F)_P^{rxn}$ held at 0·3 J/K per g should be noted.

important. A higher value of $(\partial S/\partial F)_P^{rxn}$ applies after opx exhaustion, and this may be of importance to melting or melt–rock reactions associated with dunite formation (e.g. Kelemen *et al.*, 1995).

FACTORS INFLUENCING ISOBARIC MELT PRODUCTIVITY

The isobaric melt productivity, defined as the change in melt fraction with temperature at constant pressure, $(\partial F/\partial T)_p$, enters explicitly into the expression for isentropic productivity [see equation (1)] and thus has a critical influence on the amount of melt generated from a given source region during adiabatic upwelling (McKenzie, 1984; Miller *et al.*, 1991; Langmuir *et al.*, 1992; Asimow *et al.*, 1997). MELTS calculations suggest that for melting of fertile spinel peridotite $(\partial F/\partial T)_p$ is highly variable and is affected by phase exhaustion, melt removal, and whether melting takes place near the solidus or at higher melt fractions (Hirschmann *et al.*, 1998*b*). Through equation (1), these variations in $(\partial F/\partial T)_p$ are largely responsible for the calculated variations in $(\partial F/\partial P)_S$ shown in Fig. 2. The importance of these variations can also be inferred by analogy with a rigorous thermodynamic analysis in simple systems (Asimow *et al.*, 1997).

It is commonly assumed that fractional melting is less productive than batch melting (Langmuir *et al.*, 1992; Iwamori *et al.*, 1995). The intuitive basis for this assumption in multicomponent systems is that relative to residues generated by batch melting, residues of fractional melting are more depleted in easily fusible components, so melting of fractional residues is expected to require higher temperatures. Although isobaric experiments (Hirose & Kawamura, 1994) and MELTS calculations (Hirschmann *et al.*, 1998*b*) suggest that fractional (or incremental batch) melting of the same bulk composition is indeed less productive than batch melting during the first few percent of melting, both suggest that isobaric productivities for fractional fusion can actually be comparable with or greater than those for batch fusion during later increments of melting before the exhaustion of cpx from the residue.

In this section, we analyze the principal factors influencing the variation in $(\partial F/\partial T)_p$ for batch and fractional melting, to provide insights into how productivity is likely to vary in complex peridotitic systems and how it may be affected by differences in process (batch vs fractional melting) and in source composition (enriched vs depleted peridotite). We begin by examination of a simple two-component system. Variations in productivity in this simple system show a number of interesting features relevant to understanding natural melting processes that are common to more complex systems, including peridotite. Because the simple system is more amenable to quantitative analysis, we examine these features in detail. We then examine a slightly more complex ternary system that mimics the behavior of peridotite in a semi-quantitative fashion. Finally, we use MELTS to explore variations in $(\partial F/\partial T)_p$ in model peridotite systems. Because MELTS cannot calculate true fractional melting processes, we instead calculate incremental batch melting and removal with a small step size (0·1 vol. %). A common theme in all three treatments is that variations in isobaric melt productivity can be understood in terms of changes in melt composition and that productivity variations are strongly influenced by the behavior of incompatible components present in modest abundances (in peridotite, these may include Na_2O, K_2O, H_2O, CO_2, P_2O_5, and TiO_2). Our treatment differs from that of Asimow *et al.* (1997), which emphasized changes in solid compositions and which, aalthough rigorously correct, does not lend itself as easily to an intuitive understanding of variations in $(\partial F/\partial T)_p$.

Two-component system

We first explore a two-component system composed predominantly of one component Z that forms a nearly

pure solid phase and a trace amount of a second component Y that is incompatible in that solid phase. The liquidus temperature, T, in this system can be estimated by a simple approximation of the freezing point depression relation

$$X_Y^{liq} = k(T_Z^{fus} - T) \tag{4}$$

(Denbigh, 1981, p. 261), where X_Y^{liq} is the mole fraction of component Y in the liquid, T_Z^{fus} is the melting temperature of pure solid Z, and k is a constant given by

$$k = \frac{\Delta H_Z^{fus}}{R T_Z^{fus^2}} \tag{5}$$

where ΔH_Z^{fus} is the enthalpy of fusion of pure solid Z, and R is the gas constant. It should be noted that the freezing point depression (and consequently all the effects described below) are, at the level of the approximation given by equation (4), independent of the identity of the incompatible element; i.e. on a molar basis, all incompatible elements have the same effect in the limit of zero concentration, and their effects are additive, such that X_Y^{liq} in equation (4) can signify the molar sum of all incompatible elements.

For batch melting

$$X_Y^{liq} = k(T_Z^{fus} - T) = \frac{X_Y^{bulk}}{(F + (1-F)D_Y^{*sol/liq})} \tag{6}$$

and for fractional melting

$$X_Y^{liq} = k(T_Z^{fus} - T) = \frac{X_Y^{bulk}}{D_Y^{*sol/liq}}(1-F)^{(1/D^{*sol/liq}-1)} \tag{7}$$

where X_Y^{bulk} and $D_Y^{*sol/liq}$ are the molar concentration in the bulk system and the molar partition coefficient, respectively, for the minor incompatible component Y (Shaw, 1970). Equations (4), (6), and (7) can be differentiated and solved for dF/dT:

$$\left(\frac{\partial F}{\partial T}\right)_P^{batch} = \frac{k[(1-D_Y^{*sol/liq})F + D_Y^{*sol/liq}]^2}{X_Y^{bulk}(1-D_Y^{*sol/liq})} \tag{8}$$

$$\left(\frac{\partial F}{\partial T}\right)_P = \frac{kD_Y^{*sol/liq^2}}{X_Y^{bulk}(1-D_Y^{*sol/liq})(1-F)^{(1/D_Y^{*sol/liq}-2)}}. \tag{9}$$

To illustrate the effects of incompatible elements on isobaric productivity, we use these expressions to calculate $(\partial F/\partial T)_P$ for progressive batch and fractional melting for a system where Y is incompatible ($D_Y^{*sol/liq}$ = 0·01), ΔH_Z^{fus} = 50 kJ/mol and T_Z^{fus} = 1600 K. To examine the effect of the variable concentration of the incompatible component, we calculate both batch and fractional melting for two values of X_Y^{bulk}, 0·001 and 0·002. The results are plotted in Fig. 3. Key features of the resulting trends include:

(1) As $F \to 0$ (i.e. as the solidus is approached), the curves for batch and fractional fusion of the same initial bulk composition have the same productivity. This is seen graphically in Fig. 3 and can be shown quantitatively, because as at $F \to 0$, equations (8) and (9) are equal:

$$\left(\frac{\partial F}{\partial T}\right)_P^{batch} = \left(\frac{\partial F}{\partial T}\right)_P^{fractional} = \frac{kD_Y^{*sol/liq^2}}{X_Y^{bulk}(1-D_Y^{*sol/liq})}. \tag{10}$$

(2) Systems with higher concentrations of the incompatible component Y have lower isobaric productivities at a given F for both batch and fractional processes (i.e. compare the two sets of curves in Fig. 3, for X_Y^{bulk} = 0·001 or 0·002). This is contrary to what might be assumed based on intuition; namely, that fertile sources (i.e. those rich in incompatible, easily fusible components) are usually thought to have higher productivities than depleted sources. However, the reason for the actual behavior is easy to see by inspection of equations (8) and (9): enrichments in Y cause decreases in dF/dT because X_Y^{bulk} is in the denominators of these equations.

(3) Productivity increases with increasing melt fraction (Fig. 3) for both equilibrium and fractional fusion. The rate of increase is related to the change in concentration of the incompatible component Y, as can be seen from differentiation of equation (4) with respect to F:

$$\left(\frac{\partial F}{\partial T}\right)_P = \frac{-k}{\left(\frac{\partial X_Y^{liq}}{\partial F}\right)_P} \tag{11}$$

which shows that dF/dT is inversely proportional to the change in concentration of component Y with changing F. Thus, productivity is small when the concentration in the liquid of Y in the melt changes rapidly (as it does for both batch and fractional fusion near the solidus). With increasing F, productivity increases as the concentration of Y decreases less rapidly, and levels off at higher F. Also, because changes in Y are initially more rapid for fractional fusion, near the solidus fractional fusion will be less productive than batch fusion (but right at the solidus, the productivities for the two processes are identical). This can be seen analytically by differentiation of equations (8) and (9), which gives that as $F \to 0$,

$$\frac{\partial}{\partial F}\left(\frac{\partial F}{\partial T}\right)_P^{batch} = 2\frac{kD_Y^{*sol/liq}}{X_Y^{bulk}} \tag{12}$$

and

$$\frac{\partial}{\partial F}\left(\frac{\partial F}{\partial T}\right)_P^{fractional} = (1-D_Y^{*sol/liq})\frac{kD_Y^{*sol/liq}}{X_Y^{bulk}} \tag{13}$$

Inspection of the equations shows that, from the identical

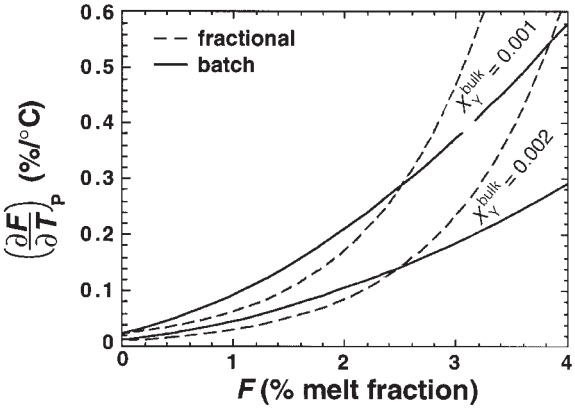

Fig. 3. Calculated isobaric productivity, $(\partial F/\partial T)_P$, for binary model described in text, consisting predominantly of one component (Z) but also containing a minor quantity of a component (Y) that is highly incompatible in the solid phase. Calculations are given for batch (solid curves) and fractional (dashed curves) melting of systems with 0·002 or 0·001 of the Y component in the initial bulk system. It should be noted that for a given composition, fractional and batch melting produce the same productivity at the solidus, fractional melting is less productive than batch melting near the solidus, and the opposite is true at higher melt fractions; also, productivity is higher for the bulk system poor in the incompatible component.

values at the solidus, the productivity for batch melting initially (i.e. at very small F) increases more rapidly than for fractional fusion because $2 > D_Y^{*sol/liq}$. This yields the expected result that fractional fusion is less productive than batch fusion. However, in this simple system, this result is valid only near the solidus: as melting proceeds, absolute changes in the concentration of Y become smaller for fractional than for batch fusion (because the concentration in the liquid for fractional fusion is nearly zero after a few percent melting), so fractional fusion becomes more productive than batch fusion as the melt fraction builds up (Fig. 3). The crossover between batch and fractional productivities is the condition

$$\left(\frac{\partial F}{\partial T}\right)_P^{batch} = \left(\frac{\partial F}{\partial T}\right)_P^{fractional} \tag{14}$$

which occurs when

$$\frac{D_Y^{*sol/liq}}{(1-F)^{(1/D_Y^{*sol/liq}-2)}} = [(1-D_Y^{*sol/liq})F + D_Y^{*sol/liq}]^2 \tag{15}$$

in other words, it depends only on $D_Y^{*sol/liq}$.

Although we shall see below that this model binary system illustrates many effects that are of general relevance to productivity variations of partially melting multicomponent system and thus allows them to be understood quantitatively and simply, it is unlike natural systems in important respects. To begin with, the residue is monomineralic so the effects of phase exhaustion on productivity are not included (see below). Also, the solid is nearly pure and its melting is approximated as congruent. Treatment of the solid as a pure, congruently melting compound leads to several inadequacies for understanding natural systems with increasing melt fraction. For example, as melting proceeds and the concentration of the Y component in the melt decreases in the melt, productivity must tend towards very high values, and for fractional melting, it tends toward infinity. To enhance our insight into productivity variations, we now examine a ternary system for which productivity is not required to go to arbitrarily high values.

Three-component system

The model ternary system predominantly consists of two components, A and B, which form a solid solution, and a small quantity of a third component, C, which is incompatible in the solid solution (Fig. 4). This ternary system more closely resembles peridotite than does the binary described above because there is a slowly varying background productivity, governed by the A–B solid solution loop (Fig. 4a), which is perturbed near the solidus by the effect of the small quantity of the incompatible component C. Component C is therefore a proxy for Na_2O in fertile peridotite or H_2O, K_2O, P_2O_5, etc. in a 'damp' and/or metasomatized peridotite. As we shall see, this system has the minimum complexity necessary to mimic the essential features of productivity during isobaric melting of peridotite in the absence of solid–solid phase changes or exhaustion of a phase from the residue.

We assume that partitioning of A and B between liquid and solid is characterized by a single equilibrium constant, K_D,

$$K_D = \frac{X_A^{liq} X_B^{sol}}{X_A^{sol} X_B^{liq}} \tag{16}$$

and that partitioning of component C is governed by Henry's Law,

$$D_C^{*sol/liq} = \frac{X_C^{sol}}{X_C^{liq}} \tag{17}$$

Heat capacities of the liquid and solid are assumed to be equal. Under these conditions, the liquidus temperature, T for any liquid can be approximated using the cryoscopic equation (e.g. Carmichael *et al.*, 1974, pp. 170–173),

$$T = \frac{\Delta H_A^{fus}}{R\left(\frac{\Delta H_A^{fus}}{R T_A^{fus}} - \ln\left(\frac{X_A^{liq}}{X_A^{sol}}\right)\right)}. \tag{18}$$

This approximation neglects the effects of the melting temperatures and ΔH^{fus} of the B and C components, but provides an adequate description of a system in which

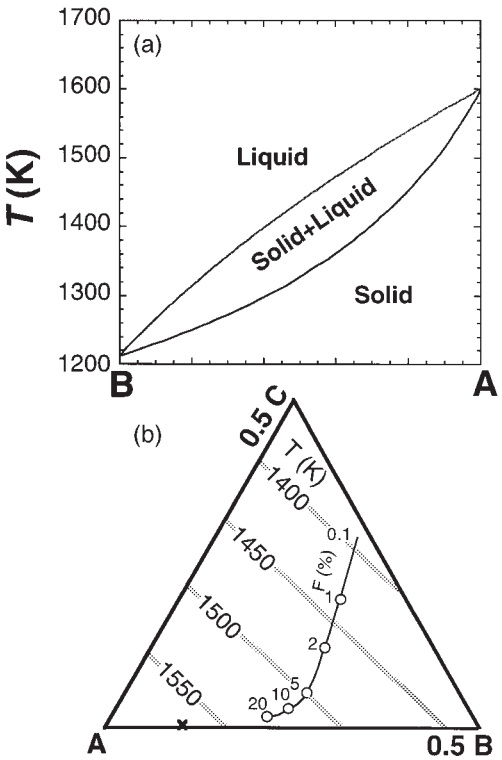

Fig. 4. Calculated phase relations for the simple model ternary described in text. (a) Calculated phase relations along the A–B join are those of a solid solution in equilibrium with an ideal partial melt. (b) The A-rich portion of the model ternary system with calculated isotherms and the calculated batch partial melt composition. The liquidus phase everywhere is the A–B solid solution, with trace quantities of dissolved C. Numbers along the trace of the partial melt curve are percent melt present. It should be noted that the distance in temperature between constant increments of melt decreases as the total amount of melt increases, illustrating that $(\partial F/\partial T)_P$ is small near the solidus and increases as melting proceeds. '×' indicates bulk system composition.

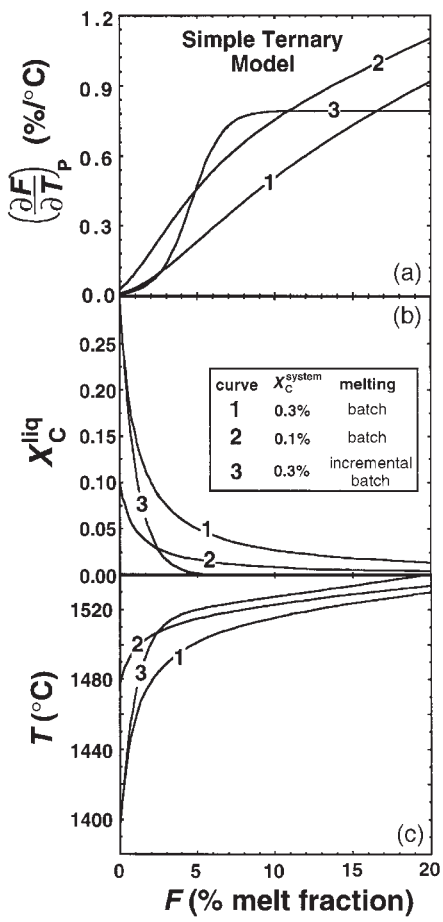

Fig. 5. Calculations of (a) isobaric productivity, $(\partial F/\partial T)_P$, (b) the concentration of incompatible component C in the liquid, and (c) temperature vs melt fraction (in percent) for the simple model ternary system described in the text and shown in Fig. 4. For each panel, calculations were performed for an initial bulk composition of 89·7 mol % A, 10% B and 0·3% C (curves labeled '1' and '3') or 89·9% A, 10% B and 0·1% C (curves labeled '2'). Curves labeled '1' and '2' are for batch melting: curves labeled '3' are for incremental batch melting, with melting steps of 0·1%.

the liquid is rich in the A component, and it is thus sufficient for our purposes. We assume values of K_D, $D^*_C{}^{sol/liq}$, ΔH_A^{fus} and T_A^{fus} of 0·3, 0·01, 50 kJ/mol, and 1600 K and a bulk composition of 89·7% A, 10% B, and 0·3% C. Given these values, the relationship between liquid composition, melt fraction, and temperature is completely described by equations (16)–(18). The calculated phase relations along the A–B join are shown in Fig. 4a, and the composition of liquids and position of isotherms in the ternary are shown in Fig. 4b. The relationships between temperature, melt composition, and melt fraction for batch and fractional fusion are illustrated by the curves labeled 1 and 3 in Fig. 5.

The calculated productivity for this ternary solution shows the same essential features as the binary solution already discussed. Comparing batch vs fractional melting, productivity is the same at the solidus, higher for batch melting near the solidus, and higher for fractional melting above a certain critical degree of melting (~2·5% melting for this example). As in the case of the binary model, the key variable is the rate of change of the liquid composition as melt fraction increases. Reflecting the phenomenon of freezing point depression, C-rich liquids formed near the solidus have low melting temperatures (Fig. 5c). However, after only small increases in melt fraction, X_C in the liquid is sharply reduced (simply because of the incompatibility of component C; Fig. 5b), and therefore the freezing point depression decreases substantially (i.e. the liquidus temperature rises substantially; Fig. 5c). Decreases in the B content of the liquid contribute much less to liquidus temperature changes near the solidus, and become important relative

to the effects of C only as C in the liquid becomes more dilute at higher melt fractions. As implied at the end of the previous section on the binary model system, an important difference is that in the ternary system the productivity does not increase to very large values, but instead levels off [i.e. $(\partial^2 F/\partial T^2)_P$ is negative rather than positive above a few percent melting]; this is particularly apparent for the fractional fusion example, where the productivity becomes nearly constant at the background level of the A–B binary once the concentration of component C becomes negligible above ~7–8% melting (as a result of which, batch fusion again becomes more productive than fractional fusion at above 16–17% melting). Thus, the generalizations in the previous section regarding productivity variations near the solidus and their causes are not artifacts of the approximation that the solid is a pure, congruently melting compound.

Although the calculated productivity at any given F is always lower for enriched sources than for depleted sources (compare curves 1 and 2 in Fig. 5a) and fractional melting is more productive than batch melting over much of the melting interval, it is important to note that the total extent of melting at any given temperature is always greatest for batch melting of the enriched source for this simple system (i.e. above the solidus, curve 1 is further to the right than the others in Fig. 5c). Thus, the total amount of melt resulting from isobaric heating is greatest for more enriched sources and for batch melting. For the comparison between enriched and depleted sources, this is because enriched sources begin to melt at a lower temperature. For the comparison between batch and fractional processes, this is because fractional melt production never 'catches up' with batch melt production, owing to its lower productivity near the solidus. These features are also seen in peridotite melting calculations, as discussed in the next section.

Isobaric melt productivity near the peridotite solidus

We now turn to MELTS calculations of isobaric productivity of fertile peridotite at 1 GPa. Calculations predict that $(\partial F/\partial T)_p$ of fertile peridotite is small near the solidus and increases as melting proceeds up to the exhaustion of cpx from the residue (Hirschmann *et al.*, 1998*b*). This is illustrated by curve 1 in Fig. 6a, which shows $(\partial F/\partial T)_p$ calculated for batch melting of MM3 peridotite at 1 GPa from the solidus up to 20% melting. The calculated $(\partial F/\partial T)_p$ increases from 0·01%/°C at the solidus to 0·6%/°C just before the exhaustion of cpx at ~18% melting. By analogy to the simple systems above, this dramatic increase in isobaric productivity reflects primarily the significant decrease in the concentration of Na in the liquid as melting proceeds with rising temperature (see curve 1 in Fig. 6b). We note again that

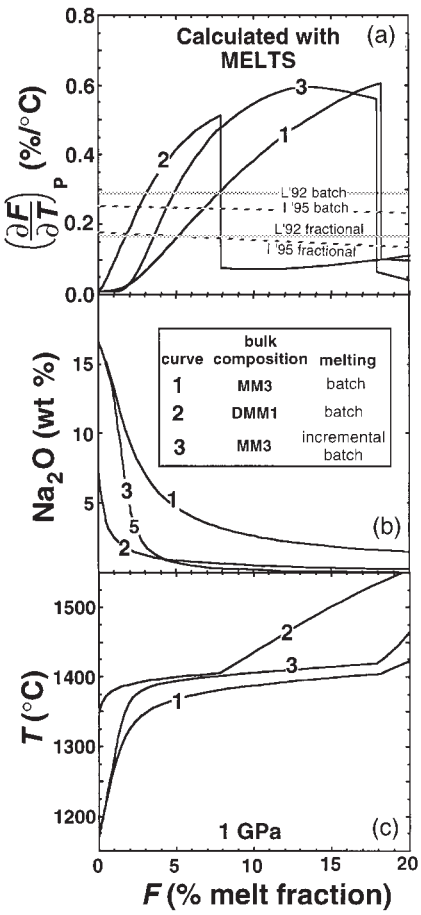

Fig. 6. MELTS calculations of (a) isobaric productivity, $(\partial F/\partial T)_P$, (b) concentration of Na_2O in the liquid, and (C) temperature vs melt fraction (in percent). In each panel, calculations are performed for batch melting of the fertile MM3 peridotite composition (curves labeled '1'), batch melting of the depleted DMM1 peridotite composition (curves labeled '2'), and incremental batch melting (i.e. an approximation to fractional fusion) of MM3, with melting steps of 0·1% (curves labeled '3'). For incremental batch melting, the productivity is calculated relative to the original source mass (Asimow *et al.*, 1997). Discontinuities in $(\partial F/\partial T)_P$ at ~18% melt (MM3) and ~8% melt (DMM1) reflect exhaustion of cpx from the solid residue. Also shown in (a) are the isobaric batch and fractional productivities calculated from the models of Langmuir *et al.* (1992) (L'92) and Iwamori *et al.* (1995) (I'95). All calculations at 1 GPa, except the trend in (a) from Iwamori, which is at 1·5 GPa.

although the change in $(\partial F/\partial T)_p$ calculated by MELTS for the MM3 composition is exaggerated because the concentration of Na_2O in calculated near-solidus liquids is too high (Hirschmann *et al.*, 1998*b*), the overall form of the effect is robust.

Because the decrease in isobaric productivity near the solidus is related to the change in the abundance of incompatible components in the melt, all other things being equal, we would predict that productivities for systems depleted in incompatible elements will be larger

than those enriched in those components; we recall that this effect was observed in our simple binary and ternary model systems (Figs 3 and 5), and an inverse proportionality between productivity and the concentration of incompatibles in the source in the binary system is apparent from inspection of equations (8) and (9). This is also the case for more complex model peridotite systems: for example, as shown in Fig. 6a, the MELTS-calculated near-solidus productivity for batch melting of the depleted DMM1 peridotite composition is higher before exhaustion of cpx at ~8% melting than that calculated for batch or for fractional fusion of the fertile MM3 peridotite composition (although the calculated productivity still increases with increasing F, reflecting again the decreasing Na content of the melt). Although it is difficult to distinguish in Fig. 6a, productivity for DMM1 is also higher than that of MM3 right at the solidus, again following the behavior observed in the model binary and ternary systems. It should be noted that, as also observed for the model ternary, the calculated temperature required to reach a given melt fraction is always higher for a depleted composition than for a fertile system for the complex peridotite compositions (Figs 5c and 6c). Thus, although the melt fraction generated from fertile peridotite at any given temperature will always be greater than for a depleted peridotite, the difference between the temperature required to generate a particular melt fraction in the depleted composition and that required to generate that same melt fraction is reduced as melt fraction increases (so long as a phase is not exhausted from the residue of either source). The key point is that owing to these variations in isobaric productivity, all other things (e.g. the phase assemblage) being equal, the initial adiabatic productivity of any given peridotite composition as it upwells past its solidus will be inversely correlated with the concentrations of moderately to highly incompatible components (chiefly alkalis and volatiles) in the peridotite.

Experimental determinations of melt fraction vs temperature for fertile peridotite do not show strong evidence for the near-solidus productivity changes predicted by MELTS or by simple system analysis. The experiments of Baker & Stolper (1994) and Baker *et al.* (1995) [T–F relations summarized by Hirschmann *et al.* (1998*b*)] and Robinson *et al.* (1998) both suggest nearly constant productivity through the lherzolite melting interval. It may be that the real effects in natural peridotite are well developed only below melt fractions of ~2–3% [the lowest melt fractions explored by the Baker *et al.* (1995) experiments] and that the difficulties inherent in using variable bulk-composition sandwich experiments to characterize the temperature–melt fraction relations in theoretical constant bulk-composition peridotite introduce significant uncertainties to the Robinson *et al.* (1998) melt fraction estimates.

The differences between batch and fractional (or incremental batch) melting of fertile peridotite are illustrated in Fig. 6. The curves labeled 3 show the calculated characteristics of isobaric, incremental batch melting of MM3 peridotite (with melt removed after 0·1% increments; this is a close approximation to fractional fusion). These curves for fractional fusion can be compared with the batch melting curves (labeled 1 in Fig. 6) for the same initial bulk composition. As expected from the simple system analogies, there is no difference between predicted productivities for batch and fractional fusion right at the solidus. However, just after the first increment of isobaric fractional melting, the concentrations of fluxing components in partial melts decrease more rapidly with F than in batch melts (Fig. 6b), and, as a consequence, temperature rises more rapidly with F, and isobaric productivity is smaller for fractional fusion than for batch fusion (Fig. 6c). This is precisely the difference between fractional and batch melting that is generally assumed, but, as already demonstrated, it is a phenomenon particular to near-solidus conditions. After ~2% melt has been removed, most of the Na (and other, more highly incompatible elements) has been removed from the system undergoing fractional fusion, so the compositions of fractional partial melts, and therefore the liquidus temperatures of those partial melts, change more slowly with F than in the case of batch partial melting (Fig. 6c). Thus, from ~2% melting to the exhaustion of cpx, the calculated productivity is higher for fractional melting than it is for batch melting (Fig. 6a), just as was observed for the model binary and ternary systems described previously (Figs 3a and 5a). Therefore, whereas the common intuition that fractional melting of peridotite is less productive than batch melting is applicable near the solidus (but not right at it) and when averaged over the entire melting interval, it does not apply at higher extents of melting. It should be noted, however, that even though the productivity for incremental batch melting is greater than that for batch melting over a large fraction of the melting interval, at any given temperature the total extent of melting achieved by fractional processes is, as emphasized above, always less than that achieved by batch processes (compare curve 3 with curve 1 in Fig. 6c). Thus, despite the higher productivity of fractional fusion above ~2% melting, according to these calculations the total melt produced by fractional melting never actually 'catches up' to that produced by batch melting.

It is remarkable that the behavior predicted by MELTS for complex model peridotite compositions matches so well those calculated for the model binary and ternary systems discussed in the previous sections (compare Figs 3, 5, and 6). This is the case even though the calculated melting of the MM3 composition involves changing phase proportions in the residue and changing concentrations

of many melt and solid components, whereas productivity variations in the model binary and ternary are due entirely and nearly entirely, respectively, to variations in the incompatible component concentration in the melt with degree of melting. The strong similarities between the calculated variations in incompatible component concentrations, melting temperatures, and $(\partial F/\partial T)_p$ for the simple binary and ternary model systems and for fertile peridotite strongly suggest that the calculated variations in productivity for both simple systems and fertile peridotite are caused by similar factors. For the particular fertile peridotite composition we have chosen, variations in Na concentrations in the liquid must be primarily responsible for the calculated behavior, although for other compositions, components such as K_2O, H_2O, P_2O_5, etc. would play the same role.

Most previous models of peridotite melting have not considered the effects of fractional fusion or the fertility of the source on melt productivity (e.g. Klein & Langmuir, 1987; McKenzie & Bickle, 1988; Kinzler & Grove, 1992; Longhi, 1992). However, two models that explicitly address the effect of melt removal on productivity are those of Langmuir *et al.* (1992) and Iwamori *et al.* (1995). Langmuir *et al.* (1992) assumed that between the solidus and exhaustion of cpx, isobaric productivity during fractional melting is half that of batch melting (Fig. 6a). Iwamori *et al.* (1995) treated fractional melting by assuming that the overall form of the isobaric melt production vs temperature curve for fractional fusion mimics that of batch melting, but that the productivity at any given extent of melting is smaller, such that the batch melting F vs T curve is 'stretched' over a larger temperature interval. From the solidus up to ~30% melting, their treatment is similar to that of Langmuir *et al.* in that the isobaric productivity function for fractional melting is nearly linear, but reduced relative to the batch melting function (Fig. 6a). However, these treatments are not consistent with (1) predictions by MELTS [Fig. 6 and Hirschmann *et al.* (1998*b*)]; (2) predictions of the simple model systems illustrated in Figs 3–5; (3) the results of incremental batch melting experiments (Hirose & Kawamura, 1994); or (4) the thermodynamic analysis presented by Asimow *et al.* (1997).

As is the case for the model binary and ternary systems described above, the peridotite melting calculations show lower calculated productivities for batch vs fractional processes and for enriched vs depleted compositions. However, as emphasized previously for these simple model systems, this does not contradict the commonsense presumption that enriched compositions will melt more than depleted compositions and that batch melting leads to more melting than fractional melting, as demonstrated by the fact that the calculated melt fraction at any given temperature is always greatest for batch melting of the enriched source (see Figs 5c and 6c). In addition, because isobaric productivities so strongly influence adiabatic productivities (Asimow *et al.*, 1997), this generalization is also likely to apply to melt production in upwelling mantle. In other words, at a given potential temperature, enriched sources will begin to melt deeper than depleted sources and fractional melting will for any composition produce less melt than batch melting near the solidus; but, as upwelling proceeds beyond a certain point, the difference in extent of melting when comparing different compositions and processes becomes smaller, rather than larger. A detailed evaluation of the effect of productivity variations in fractional and batch partial melting of peridotite during adiabatic melting is in preparation (Asimow *et al.*, 1999).

The effects of cpx exhaustion on peridotite melting

When cpx is exhausted from the residue during isobaric batch melting of spinel peridotite at 1 GPa, the isobaric productivity calculated by MELTS decreases by more than a factor of four [Fig. 6 and Hirschmann *et al.* (1998*b*)]. In general, there will be a discontinuous drop in productivity when a phase is exhausted from the residue, resulting from the discontinuous decrease in the temperature derivative of the bulk solid composition that occurs when the melting reaction changes (Asimow *et al.*, 1997). The decrease in this derivative decreases isobaric productivity by analogy with the rigorous result for binary systems, in which lever rule considerations require that the isobaric productivity is approximately proportional to the change in bulk solid composition (Asimow *et al.*, 1997). For the specific case of peridotite melting, the drop in productivity accompanying exhaustion of cpx reflects the change from a melting reaction dominated by cpx melting to one dominated by opx melting (Hirschmann *et al.*, 1998*b*). MELTS also predicts that isobaric melt production following cpx exhaustion is less for fractional melting than for batch melting (Fig. 6a). This prediction must be qualitatively correct, as can be proved from theoretical constraints developed from simple systems (Presnall, 1969; Asimow *et al.*, 1997).

The decrease in isobaric productivity associated with cpx exhaustion translates into lower adiabatic productivities following elimination of cpx from the residues of upwelling peridotite (Asimow *et al.*, 1997). This abrupt decrease in productivity may influence the distribution of porosity (and hence, permeability) across the cpx-out boundary, and this may influence the flow and segregation of melt in upwelling mantle (Spiegelman, 1993; Asimow *et al.*, 1995). Although melting of upwelling peridotite would generally be expected to continue at lower productivity after the exhaustion of cpx (provided, of course, that adiabatic upwelling is not interrupted by

the base of the lithosphere), the maximum extent of melting in mid-ocean ridge basalt (MORB) source regions, as represented by abyssal peridotites, is commonly just past that required to exhaust cpx (Dick *et al.*, 1984), and this may reflect the decrease in productivity beyond cpx-out. Thus, particularly if melting is near-fractional, there could be shallow regions beneath mid-ocean ridges (and ocean islands) that have adiabatic geotherms but that do not produce appreciable volumes of melt. Better quantification of the magnitude of this effect is needed, particularly because models that call on mantle temperature as the key variable controlling crustal thickness and that rely on passive upwelling (McKenzie & Bickle, 1988; Langmuir *et al.*, 1992) require significant melting of harzburgite to account for regions of very thick crust, such as near Iceland. These models may require re-examination if productivity of fractional melting following exhaustion of cpx is as significantly reduced as predicted by MELTS.

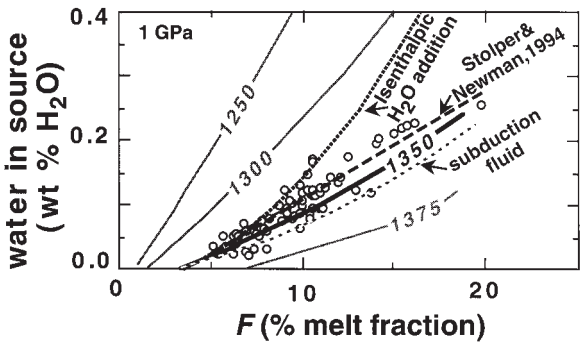

Fig. 7. MELTS calculation of the effects on melting of addition of H_2O to hot (1250, 1300, 1350 and 1375°C), fertile MM3 peridotite at 1 GPa. Circles are extent of melting and water-in-source inferred for Mariana trough basalts by Stolper & Newman (1994); the dashed line is their best fit line to these points. It should be noted that the Stolper & Newman trend is nearly identical to the calculated isothermal trend at 1350°C. Also shown are trends for isenthalpic addition of H_2O to anhydrous MM3 peridotite initially at 1350°C (heavy dotted curve) and isothermal addition of a model subduction fluid (45 wt % H_2O, 45 wt % Na_2O, 10 wt % K_2O; spaced dotted curve) to the same peridotite composition. Compared with isothermal addition of H_2O, isenthalpic addition results in less melting. Compared with pure H_2O, addition of the subduction fluid results in a modest increase in the melt generated per increment of H_2O added.

MELTING OF HYDROUS PERIDOTITE

In considering the effects of H_2O on peridotite partial melting, we will examine two scenarios. First, we investigate the isobaric case where increments of H_2O are added to hot peridotite, at which point melting is allowed to proceed either adiabatically or isothermally at constant pressure. This approximates the situation that probably occurs above subduction zones, where water [and probably significant quantities of alkalis (Stolper & Newman, 1994)] from the dehydrating slab is added to the overlying wedge (e.g. Gill, 1981). Second, we examine the case where peridotite with a fixed amount of H_2O melts in response to isobaric heating. As described above, the isobaric productivity is an important constraint on adiabatic melting behavior, so this second example has relevance to melting of water-bearing peridotite in response to upwelling in sub-arc regions or elsewhere.

Effects of H_2O addition on melting under isothermal or isenthalpic conditions

Isothermal melting

Incremental addition of water to hot peridotite under isothermal, isobaric conditions results in significant increases in the amount of melt present (Fig. 7). MELTS predicts that the increase in melt fraction per increment of water, $(\partial F/\partial C^{\text{bulk}}_{\text{H}_2\text{O}})_{\text{T,P}}$ (where $C^{\text{bulk}}_{\text{H}_2\text{O}}$ is wt % H_2O) is approximately constant at a given P and T up to the exhaustion of cpx. The rate of increase is greater when temperature is high, as also surmised by Stolper & Newman (1994), Hirose & Kawamoto (1995), and Gaetani & Grove (1998). For example, at 1 GPa and 1250°C under anhydrous conditions, the calculated value of $(\partial F/\partial C^{\text{bulk}}_{\text{H}_2\text{O}})_{\text{T,P}}$ up to exhaustion of cpx is ~20%/wt %; in contrast, the calculated value at 1375°C is ~80%/wt %. Following exhaustion of cpx, the calculated $(\partial F/\partial C^{\text{bulk}}_{\text{H}_2\text{O}})_{\text{T,P}}$ drops dramatically (e.g. to between 10 and 20%/wt % at 1350°C).

The linearity of $(\partial F/\partial C^{\text{bulk}}_{\text{H}_2\text{O}})_{\text{T,P}}$ in the lherzolite region and its dependence on temperature are features reminiscent of the expected behavior of a simple two-component system such as that discussed in the isobaric productivity section above. If water is perfectly incompatible ($D^{\text{sol/liq}}_{\text{H}_2\text{O}} = 0$), then for a binary system, equation (6) gives (and applying mass units rather than molar units) $(\partial F/\partial C^{\text{bulk}}_{\text{H}_2\text{O}})_{\text{T,P}} = 1/C^{\text{liq}}_{\text{H}_2\text{O}}$. In this case, $C^{\text{liq}}_{\text{H}_2\text{O}}$ is a constant at a given temperature and pressure, as it is fixed by the location of the liquidus. Therefore, variations in $C^{\text{bulk}}_{\text{H}_2\text{O}}$ cause changes in F at a constant rate, dictated by the lever rule. Also, $(\partial F/\partial C^{\text{bulk}}_{\text{H}_2\text{O}})_{\text{T,P}}$ increases with temperature, as [from equation (4)] $(\partial C^{\text{liq}}_{\text{H}_2\text{O}}/\partial T)_{\text{T,P}} = -k < 0$, so $C^{\text{liq}}_{\text{H}_2\text{O}}$ decreases, and $(\partial F/\partial C^{\text{bulk}}_{\text{H}_2\text{O}})_{\text{T,P}}$ therefore increases with rising T. In a more complex system, $C^{\text{liq}}_{\text{H}_2\text{O}}$ will not typically be a constant at a given P and T as water is added to the system [and indeed, it is not constant in either the MELTS calculations or experiments adding water to peridotite (Hirose & Kawamoto (1995)], and this might be expected to cause deviations from a constant

value for $(\partial F/\partial C^{bulk}_{H_2O})_{T,P}$. For example, MELTS calculations and the experiments of Hirose & Kawamoto (1995) suggest that $(\partial C^{liq}_{H_2O}/\partial C^{bulk}_{H_2O})_{T,P}$ is positive for peridotite melting experiments. However, $(\partial C^{liq}_{Na_2O}/\partial C^{bulk}_{H_2O})_{T,P}$ is negative (because addition of H_2O at constant T increases melt fraction and therefore Na in the liquid is diluted). So, the effect of increasing H_2O on melt fraction (based on the lever rule) is partially countered by the effect of decrease of Na_2O, perhaps accounting for the approximate linearity of the F vs bulk water content relationships calculated by MELTS, despite the variable water content of the liquid.

The calculated isothermal trend (Fig. 7) at 1350°C, 1 GPa is in excellent agreement with the predicted effect of water addition on peridotite melting derived by Stolper & Newman (1994) from an analysis of water and trace element contents of submarine lavas from the Mariana trough. It should be noted that temperatures calculated by MELTS are typically ~100°C too high (Hirschmann *et al.*, 1998*b*), so the actual correspondence would more probably be to a 1250°C isotherm. A key inference of Stolper & Newman was that the amount of melting caused by water addition is approximately linearly related to the quantity of water added, but there were no experimental or theoretical treatments of the effect of water on the amount of melting of peridotite, so there was no way to evaluate if this was realistic. Figure 7 shows that MELTS calculations independently predict a nearly linear relationship over the interval from 0% added H_2O until the exhaustion of cpx. In addition, as described above, MELTS calculations and experiments (Hirose & Kawamoto, 1995; Gaetani & Grove, 1998) also support Stolper & Newman's statement that the amount of melt generated per increment of added H_2O is a strong function of initial temperature. Consequently, an analysis similar to Stolper & Newman's for mantle wedges markedly colder or hotter than that beneath the Mariana trough would be expected to yield very different H_2O vs F trend, and this could ultimately provide a measure of source region temperature for back-arc and arc lavas.

The preceding calculations were performed by adding pure H_2O to peridotite, but it is more likely that the fluid added to peridotite in sub-arc regions is an alkali-rich hydrous fluid (Stolper & Newman, 1994), and these added alkalis are also expected to flux the peridotite, leading to increased melting. Therefore it may not be appropriate to compare these MELTS calculations with the melt fraction vs H_2O trends inferred from natural basalt glasses. For basalts erupting in the Mariana trough, Stolper & Newman (1994) inferred that the added subduction component fluid consists of 44·1% H_2O, 42·6% Na_2O, 8·5% K_2O, with minor amounts of P and Cl. Components such as SiO_2, Al_2O_3, etc. could also be present, but their concentrations were not constrained by Stolper & Newman (1994). In Fig. 7 we show the calculated effect of adding a similar subduction component (45 wt % H_2O, 45 wt % Na_2O, 10 wt % K_2O) to peridotite at 1350°C. Compared with addition of pure H_2O under the same conditions, the subduction fluid generates only slightly greater melt per increment of H_2O added. For example, for 0·2 wt % pure H_2O added at 1350°C and 1 GPa, the calculated melt fraction is 17%. At the same temperature and pressure, adding the same quantity of H_2O in a subduction fluid (and therefore also adding 0·2 wt % Na_2O and 0·045 wt % K_2O) results in a calculated melt fraction of 18% (Fig. 7).

These calculations suggest that it is mainly the H_2O in subduction fluids that causes melting, and that the concentrations of alkalis and other dissolved metals have relatively little effect on the amount of melt produced. The model for melt fraction as a function of temperature and melt composition constructed by Gaetani & Grove (1998) suggests a somewhat larger role for the alkalis in subduction fluids; e.g. at 1330°C and 1·5 GPa, Gaetani & Grove calculated that peridotite with 0·3 wt % H_2O will be 7% molten, but that addition of a subduction fluid containing the same quantity of H_2O and attendant alkalis will lead to 10% melting under the same conditions. Gaetani & Grove concluded that the trend of Stolper & Newman (1994) can only be matched at reasonable temperature if the effects of alkalis are considered. The predominant effect of H_2O relative to alkalis in the MELTS calculations can be rationalized by the much smaller molecular weight of H_2O, as the increase in melt is affected primarily by the number of moles, rather than the mass of flux; e.g. the assumed subduction fluid on a molecular basis is 75% H_2O, 22 mol % Na_2O, 3 mol % K_2O. Additionally, relative to H_2O (or K_2O), Na_2O should have less of a stabilizing effect on melt relative to minerals because some Na_2O is incorporated in minerals. Nevertheless, additional work is required to determine whether the MELTS calculations of the effects on melt formation of water and dissolved alkalis are more or less accurate than those of Gaetani & Grove (1998).

Isenthalpic melting

The preceding discussion evaluates the effect of water addition on melt fraction at a fixed temperature. This comparison is relevant to melting processes above subduction zones if the temperature of a partially molten peridotite at a particular depth is independent of its water content. However, melting is an endothermic process, so unless the temperature is imposed externally, by conduction from a larger body of refractory rock not undergoing melting into a smaller body where melting occurs (Hirschmann & Stolper, 1996), or internally, by buffering of a nearly isothermal melting reaction such as amphibole dehydration (Wyllie, 1979), peridotites that melt more

because of an influx of water can be expected to be cooler because of the larger amounts of latent heat consumed by melting. We now consider the case in which water is added to the source, leading to isobaric, adiabatic melting. Melting under these conditions will be an isenthalpic process, and less melt will form than under isothermal conditions for the same bulk composition at the same initial temperature.

Isenthalpic addition of water is calculated using the algorithms of Ghiorso & Kelemen (1987). In these calculations, the temperature of the added water is taken to be the same as the initial temperature of the peridotite, but variation of this temperature has little effect, as resulting variations in enthalpy are small relative to the enthalpic effect of the melting reactions that result from addition of the water. Isenthalpic, isobaric addition of water to peridotite results in considerably less melting per increment of water added than the isothermal, isobaric melting calculations presented above. For example, for dry peridotite initially at 1350°C and 1 GPa, the calculated F increases from 3% to ~17% on isenthalpic addition of 0·4% H_2O, whereas under isothermal conditions, addition of less than 0·2% H_2O would be required to achieve the same melt fraction. Isenthalpic addition of water also results in considerable cooling of the peridotite, as the latent heat required to generate melt is absorbed from the thermal energy of the system. For the same example of addition of 0·4% H_2O, the resultant melting is calculated to cool the initially anhydrous peridotite by ~45°C (Fig. 7).

Whether melting of variably hydrated peridotite above subduction zones is best approximated as an isothermal, isenthalpic, or isentropic process depends on the physical melting process that is envisioned. Although the natural processes that lead to melt production in the mantle wedge overlying a subduction zone are not likely to be simply categorized, the observations of Stolper & Newman (1994), when compared with MELTS calculations and with the experiments of Hirose & Kawamoto (1995), suggest that peridotites in the source regions of the Mariana trough experience variable extents of melting as a result of variable water contents in a process that is more nearly isothermal than isenthalpic. In other words, the correspondence of the water–melt fraction trend of Stolper & Newman (1994) to a single calculated isotherm at 1 GPa suggests that temperature in the source regions of Marianas trough lavas is not internally buffered by melting reactions. This suggests that temperatures are externally imposed, possibly because length scale variations in degree of peridotite hydration are small compared with length scales over which thermal diffusion is effective (Hirschmann & Stolper, 1996; Hirschmann *et al.*, 1999).

Effects of small amounts of H_2O on melting owing to isobaric heating

Compared with anhydrous melting, addition of small amounts of H_2O to peridotite greatly lowers the initial melting temperature (Wyllie, 1979), as was simulated above in the model ternary by the addition of the incompatible component C. It should be noted that to first order, at low concentrations, all incompatible components (on a molar basis and assuming that the D values are comparable) will produce the same 'freezing point depression'; this follows from simple thermodynamics [equation (4)], and indicates that addition of a given molar fraction of H_2O, K_2O, P_2O_5, etc. will have a similar quantitative effect. In this section we explore this near-solidus effect quantitatively using MELTS calculations. These calculations indicate that addition of small amounts of water (0·1 or 0·2 wt %) to the fertile MM3 peridotite composition at 1 GPa results in the formation of small amounts (up to ~2%) of melt well below the dry solidus but that higher melt fractions are not predicted until temperatures close to those required for generating significant melt for the same anhydrous peridotite (Fig. 8). For wet peridotite with limited amounts of water, isobaric melt productivities remain small (i.e. comparable with those for near-solidus anhydrous peridotite) until the temperature where the melt fraction in the anhydrous case is >1%; for example, at a temperature where the melt fraction is small (~1%) for the anhydrous case, the calculated melt fractions for 0·1% and 0·2% H_2O added are only 3% and 6%. The experiments of Hirose & Kawamoto (1995) also suggest that for small amounts of added water, the melt fraction is limited at and below the dry solidus, although not to the extent indicated by these MELTS calculations. For example, for 0·2% H_2O added, at the temperature near (<50°C) the nominal anhydrous KLB-1 solidus (Hirose & Kushiro, 1993) at 1 GPa, their experiments indicate a melt fraction of 12%. However, Hirose & Kawamoto (1995) noted that their estimation method yields overestimates of melt fractions. The model of Gaetani & Grove (1998), based on water-bearing crystallization experiments, is closer to our predictions, suggesting that the melt fraction of a moderately hydrous (0·5 wt % H_2O) mantle will not exceed 3% until the temperature of the dry solidus is reached.

A corollary of the low melt fractions calculated near the dry solidus is that substantial water contents are required to generate high melt fractions if the temperature is below the wet solidus. This can be seen by examining the calculated 1250°C isotherm in Fig. 7. Under dry conditions, this isotherm is above the solidus, and yet with 0·4% wt % H_2O added, the melt fraction is <10%. This calculation suggests that achieving melt fractions >10% requires substantial amounts of H_2O or temperatures in excess of the dry solidus. Given that the maximum extent of melting in arcs approaches 20% (Gill, 1981; McCulloch & Gamble,

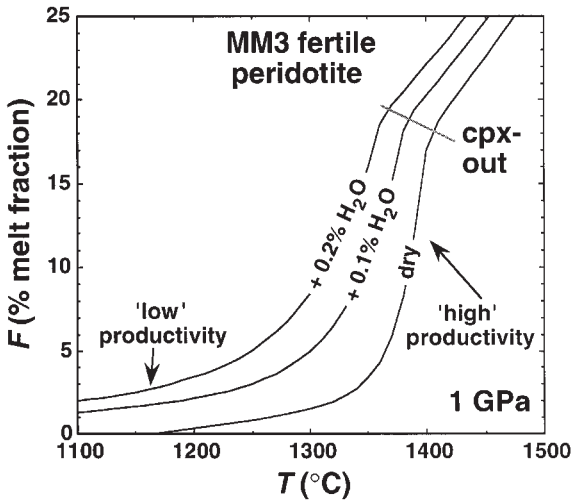

Fig. 8. Calculated effect of small fixed amount of H_2O on melting during isobaric heating for MM3 peridotite at 1 GPa. Compared with melting of anhydrous peridotite, small amounts of water significantly lower the temperature at which small melt fractions form; however, for peridotite plus these small quantities of water, melt fractions of more than a few percent are not generated until the temperature where significant (>~1%) melt is formed from dry peridotite.

1991; Stolper & Newman, 1994; Herrstrom, 1998), this suggests either that temperatures exceed the dry solidus beneath arcs [and therefore that upwelling occurs (e.g. Plank & Langmuir, 1988; Sisson & Bronto, 1998)]or that there is a mechanism for adding near-percent levels of H_2O to wedge source regions.

These inferences can be understood in terms of the relationship between melt fraction and the concentrations of H_2O and of other fluxing components in the liquid developed and analyzed above for the simple model ternary. When the melt fraction is small, the concentration of H_2O and other fluxing components (chiefly Na_2O) in the liquid is large, and the liquidus temperature is consequently low (i.e. there is a large 'freezing-point depression'). However, increases in the melt fraction sharply dilute both H_2O and other fluxing components, which requires large rises in liquidus temperature (i.e. less 'freezing-point depression'). Although relatively modest concentrations of H_2O reduce the liquidus temperature of the partial melt by a large amount, large melt fractions would also dilute the concentration of anhydrous fluxing components (e.g. alkalis), which would partially offset the effect of water on the liquidus temperature. Thus, formation of large fractions (~10%) of melt is not possible until temperatures are sufficiently high so that liquids poor in both H_2O and Na_2O are stable in equilibrium with the peridotite mineral assemblage—in other words, temperatures close to or above the dry solidus.

These calculations and experimental results contrast with the model of Iwamori *et al.* (1995), which predicts that small amounts of water cause significant melting below the dry solidus. For example, at their predicted dry solidus temperature of a fertile peridotite at 1 GPa, Iwamori *et al.* (1995) calculated that the extent of melting for peridotite with 0·2% water is ~30% (compared with ~2–3% from a similar MELTS calculation; Fig. 8). Iwamori *et al.* estimated the effect of H_2O on melting by examining the location of the wet solidus and assuming that (as for dry peridotite) the extent of melting is primarily a function of the temperature above the wet solidus, without accounting for the effect of dilution of H_2O in the melt. If correct, this would suggest that small amounts of water could cause huge increases in the volume of melt formed in the mantle. For example, Iwamori *et al.* predicted generation of 5 km of basaltic crust for adiabatic upwelling of dry peridotite with a potential temperature of 1300°C, but generation of 32 km of crust at the same potential temperature with 0·2% H_2O added. However, because increases in melt fraction are inhibited by strong dilution of H_2O in the liquid, which in turn would have a negative feedback on melt fraction at a given temperature, this probably represents a significant overestimate of increased melt production caused by a limited quantity of H_2O, and the quantitative results of Iwamori's models for hydrous peridotite must be viewed with caution.

Iwamori (1997*a*, 1997*b*) also suggested that a volumetrically important component of arc magmatism could be generated by addition to the overlying mantle wedge of water produced by decomposition of amphibole as it is pressurized during downward flow of the region of the mantle wedge overlying the slab. Some melting may indeed occur by this mechanism, though it depends on a specific confluence of thermal regime, mantle flow, and limits of amphibole stability that may be difficult to achieve in actual sub-arc regions. However, our results suggest that this process cannot produce directly large volumes of melt unless the quantity of water carried by amphibole peridotite is also very large [although it could initiate melting, leading to buoyant regions that then melt more extensively during decompression (e.g. Plank & Langmuir, 1988)]. Based on the model of Iwamori *et al.* (1995), Iwamori (1997*a*) assumed that extensive (~10%) melting of a peridotite containing 0·2 wt % total H_2O (corresponding to ~10 modal % amphibole) can take place at conditions prevailing during the breakdown of amphibole, above 2·8 GPa and near 1100°C. This is ~400°C below the dry solidus at this pressure (Takahashi *et al.*, 1993), and within ~100°C of the wet solidus (Green, 1973). Our modeling suggests that melting will not be anywhere near so extensive under these conditions. More generally, melt formation near the wet solidus requires a water activity (a_{H_2O}) near unity, whereas formation of melt near the dry solidus is possible at $a_{H_2O} = 0$. Because the solubility of water in silicate liquid is ~20 wt % at 2·8 (Eggler & Rosenhauer, 1978), a peridotite with 0·2 wt % H_2O will only produce

~1% melt at its wet solidus and melt fractions higher than ~1% will have much less dissolved water and therefore substantially lower a_{H_2O} (e.g. a 10% melt will have 2 wt % H_2O). The relationship between temperature and the a_{H_2O} required to stabilize melt between the wet and dry solidi is not known precisely, but at temperatures far from the dry solidus large values of a_{H_2O} should be necessary. Thus, the maximum extent of melting generated along the temperature–pressure path invoked by Iwamori (1997*a*) will not be much greater than 1%, about an order of magnitude less than predicted by the model of Iwamori *et al.* (1995), and far too low to account for the volumetric (e.g. Gill, 1981) or trace element (e.g. McCulloch & Gamble, 1991) characteristics of typical arc magmas.

EARLY MELT PRODUCTION DURING ADIABATIC UPWELLING

Because highly incompatible elements are most concentrated in near-solidus melts, the geochemistry of mantle melts will be strongly influenced by the conditions prevalent during the first few percent of melting. Calculations presented above and by Asimow *et al.* (1997) suggest that for adiabatic upwelling of fertile anhydrous peridotite, productivity is small during the initial stages of melting and increases continuously with increasing degrees of melting, reaching values a factor of 10 or more higher when melt fractions sufficient to exhaust cpx from the residue are achieved. The productivities calculated in this work for fertile (but K-free and volatile-free) peridotite are undoubtedly smaller than the actual expected behavior (because of the tendency of MELTS to make Na too incompatible), but small amounts of K and volatiles contained in real peridotites will further accentuate low productivity at near-solidus conditions.

Conceptually we envision two regimes, shown in Fig. 9: an 'initial melting regime' in which small amounts of melt are generated at low rates per increment of upwelling and a shallower 'major melting regime', in which productivity is markedly higher (Hirschmann *et al.*, 1994; Kinzler, 1997). The compositions of melts generated in the initial melting regime will differ substantially from those generated in the major melting regime. Important differences are that the deeper melts will be dramatically richer in alkalis and water. Although alkali enrichment in near-solidus melts is reduced as pressure increases [because of increasing compatibility of Na in cpx (e.g. Blundy *et al.*, 1995)], a 1% melt of fertile peridotite (0·33 wt % Na_2O, 0·03 wt % K_2O) at 3 GPa is still expected to contain ~7 wt % total alkalis (Hirschmann *et al.*, 1998*a*); an important consequence of this is that mineral–melt partition coefficients for highly charged trace elements (e.g. Ti, Hf, Zr, REE, etc.) are likely to be substantially different in the two regimes owing to the predicted (and observed in the case of Ti) effects of such high alkali contents on their partitioning (Blundy *et al.*, 1998; Hirschmann *et al.*, 1999).

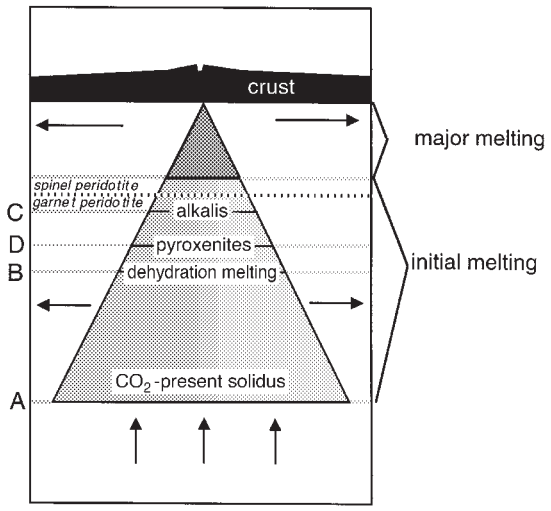

Fig. 9. Schematic depiction of melting for a region of upwelling mantle beneath mid-ocean ridges. Upwelling is assumed to be passive and the melting regime to be triangular (Plank & Langmuir, 1992). The zone undergoing melting can be divided into shallower 'major melting' and deeper 'initial melting' regimes. The boundary between these zones occurs when peridotite has melted to a sufficient extent that adiabatic productivity reaches a value that typifies melting of lherzolite through much of its melting interval, perhaps 0·3–0·4%/km. In this scheme, it is assumed that this occurs within the stability field of spinel peridotite. The initial melting regime consists of several sub-regimes. Regime A: onset of decarbonation melting leading to formation of small degree melts containing $CO_2 \pm H_2O$, as envisioned by Plank & Langmuir (1992). Regime B: onset of melting in response to dehydration of nominally anhydrous phases, as suggested by Hirth & Kohlstedt (1996). Regime C: formation of small-degree alkali-rich melts (Hirschmann *et al.*, 1994; Kinzler, 1997; this work). Regime D: initial melting of olivine-poor heterogeneities such as garnet pyroxenites, as described by Hirschmann & Stolper (1996). The relative dimensions of the various sub-regimes are not well constrained. The depth of initial melting in Regime D may be shallower or deeper than in Regime C.

The thickness of the deeper, low-productivity melting regime depicted in Fig. 9 is somewhat arbitrary, but for fertile peridotite compositions there is a rapid transition from low to high productivity in the calculated melt fraction vs pressure curve for isentropic melting at 2–5% melting [see fig. 7c and d of Asimow *et al.* (1997); the equivalent transition in the isobaric productivity for fertile, dry peridotite at a similar melt fraction can be seen in Fig. 8 of this paper]. Although the pressure difference between the solidus and this transition during isentropic ascent depends on composition and potential temperature, the typical pressure interval for fertile peridotite based on MELTS calculations is 10–15 kbar, corresponding to a 30–45 km thickness for the low-productivity zone. Hirth & Kohlstedt (1996) reached a similar conclusion for the effects of water alone: they estimated that 50 ppm H_2O dissolved in olivine can

cause melting to initiate 20–40 km deeper than melting of dry peridotite along the same adiabat.

There are probably several distinct sub-regimes within the deeper, low-productivity zone for fertile peridotite (Fig. 9):

(1) The deepest sub-regime, assuming that carbon in peridotite resides in carbonates, graphite, diamond, or a fluid (i.e. not primarily as a minor substituent in silicates), would be controlled by melting at the $CO_2 \pm H_2O$-vapor (or fluid)-saturated solidus (Regime A in Fig. 9) (Plank & Langmuir, 1992), though the location of this solidus is imperfectly constrained (Wyllie, 1979; Olafsson & Eggler, 1983; Canil & Scarfe, 1990). Nearly all of the CO_2 in the source would partition into the melt at the base of this zone, and the amount of melt would increase very slowly (i.e. the productivity would be very low) as generally expected for highly incompatible elements that effect large freezing point depressions (as per the isobaric productivity discussion above).

(2) Because of the high solubility of hydrogen in silicate minerals at high pressure (Hirth & Kohlstedt, 1996; Kohlstedt *et al.*, 1996), little of the water dissolved in olivine and other silicates will go into the melt in Regime A. Most of the water will be expelled from the peridotite by melting in an intermediate regime caused by dehydration of olivine and other silicates, as suggested by Hirth & Kohlstedt (1996) (Regime B in Fig. 9). Productivity will increase in this regime relative to the values in the deeper zone, but it will still be very small given the low water and carbon dioxide contents of the melt and the still large freezing point depression. It should be noted that initial productivities would be high if there were a water-rich fluid present (Gaetani & Grove, 1998), as may be the case for water-initiated melting in some arc environments.

(3) The shallowest sub-regime of the deep, low-productivity zone is associated with the formation of high-alkali silicate melts. This regime corresponds to the low-productivity tail calculated by us and Asimow *et al.* (1997) for anhydrous peridotite; it is predicted to extend to within a few tens of kilometers of the major-melting regime (Regime C in Fig. 9).

(4) Although of somewhat different origin, behavior, and consequences, a fourth regime beginning deeper than the peridotite major-melting regime may be generated by partial melting of pyroxene-rich mantle heterogeneities (Hirschmann & Stolper, 1996) (Regime D in Fig. 9).

The relative thicknesses of these regimes are poorly known and probably rather variable depending on source composition; the placement of Regime D in Fig. 9 relative to that of the other regimes is arbitrary.

The geochemical consequences of deep, low-productivity melting regimes in MORB source regions have been discussed previously by Plank & Langmuir (1992), Hirschmann & Stolper (1996), and Hirth & Kohlstedt (1996). Although we will not discuss it in detail here, we note that initial melting regimes are also likely to be present in OIB and supra-subduction zone environments, where incompatible-component (alkali, H_2O, CO_2)-enriched peridotite is likely to be present, and therefore that geochemical affects related to such regimes are likely to be present in these other environments.

Hirschmann & Stolper (1996) and Hirth & Kohlstedt (1996) emphasized the potential role of such regimes in imparting garnet signatures to MORB. In particular, such melting regimes can play an important role in the development of U-series disequilibria in mantle-derived melts. U-series disequilibria are expected to be strongly influenced by mantle melting processes in the initial melting regime because, owing to the highly incompatible behavior of U, Th, Pa, and Ra, fractionations among these elements can only occur at very low melt fractions. U-series disequilibria are also enhanced by low productivities because their generation is rate dependent (McKenzie, 1985). For example, for a deep melting zone that extends for 40 km, over which only 1% melt is generated (as is likely in Regimes A, B, and possibly C in Fig. 9), the average adiabatic productivity is 0·025%/km, more than an order of magnitude smaller than that expected in the shallower major melting regime. With this productivity and assuming an upwelling rate of 3 cm/year, application of a dynamic melting model (McKenzie, 1985; Williams & Gill, 1989), the partition coefficients of Beattie (1993), and the peridotite melting regime specified in fig. 6 of Hirschmann & Stolper (1996), $(^{230}Th)/(^{238}U)$ of the integrated melt would be 1·10 for adiabatic productivities representative of the major melting regime (0·33%/km), but 1·54 for a productivity of 0·025%/km. Even for an upwelling rate of 10 cm/year, melting in this deep, low-productivity regime could produce $(^{230}Th)/(^{238}U)$ as high as 1·29. Most MORB have $(^{230}Th)/(^{238}U) < 1{\cdot}3$ [see compilation by LaTourrette *et al.* (1993)], suggesting that melting in such low-productivity regimes can account for much or all of the observed $(^{230}Th)/(^{238}U)$ disequilibria in MORB. If melt transport is taken into account (Spiegelman & Elliott, 1993), the effect of deep, low-productivity zones on U-series disequilibria is probably lessened because melt transport in these zones is expected to be relatively slow (although the rates and mechanisms of melt transport in these zones are poorly known), thereby allowing for enhanced decay of daughter nuclei (e.g. ^{230}Th) during melt transport.

Our analysis of isobaric melt productivity above shows that for initial melting regimes B and C, where melting is caused by formation of melts rich in incompatible components (H_2O and alkalis, respectively), initial productivity will be lowest for those compositions with the highest enrichments in those components. If such enrichments correlate with other geochemical indicators of enrichments (e.g. trace element abundances and ratios)

then one might expect that larger U-series disequilibria would be generated in geochemically enriched regions, and such a correlation has been identified for globally averaged MORB (Bourdon *et al.*, 1996). It should be noted that this correlation between enrichment and low adiabatic productivity is the opposite of that expected if the enrichment is contained within isolated enriched pockets or veins that, as they melt as part of a regional upwelling, equilibrate thermally with the surrounding, less fertile mantle (e.g. Hirschmann & Stolper, 1996). Also, it should be noted that such a correlation can depend on the distribution of heterogeneities, as small regions of enriched peridotite may have high effective productivities owing to diffusive heating from surrounding less enriched rocks (Sleep, 1984; Hirschmann & Stolper, 1996; Hirschmann *et al.*, 1999), but on average, regions with greater concentrations of incompatible components are expected to have lower initial productivities.

CONCLUSIONS

(1) The variable relating melt productivity to the redistribution of entropy within a multicomponent system is $(\partial S/\partial F)_P^{rxn}$, the isobaric entropy change of the melting reaction, not ΔS^{fus}, which is poorly defined in such systems. Evaluation of $(\partial S/\partial F)_P^{rxn}$ must account for differences in specific entropies of minerals and melts and for the stoichiometry of the instantaneous melting reaction. $(\partial S/\partial F)_P^{rxn}$ varies with temperature, the extent of melting, and the character of the residual mineral assemblage; it is largest near the solidus and smallest when the residual solids are harzburgitic. However, adiabatic productivities are not strongly affected by these variations and a reasonable approximate value to use for $(\partial S/\partial F)_P^{rxn}$ for melting of peridotite based on MELTS calculations is 0·3 J/K per g.

(2) MELTS calculations predict that isobaric melt production near the solidus of fertile peridotite will be dramatically smaller than that at higher melt fraction. Although the magnitude of this change in productivity is exaggerated owing to imperfections in the MELTS calculation, calculations in simple model binary and ternary systems show that low productivity near the solidus is a generally expected phenomenon for sources containing quantities of strongly incompatible component sufficient to produce a 'freezing-point depression'. At any given melt fraction and assuming the same residual mineral assemblage, isobaric productivity for depleted peridotite is greater than for fertile peridotite, although the melt fraction present (for batch processes) or previously extracted (for fractional processes) at the same temperature and pressure will always be greater for the fertile peridotite.

(3) Fractional melting is less productive than batch melting near the solidus because the compositions (and therefore the liquidus temperature) of fractional melts change more rapidly than those of batch melts in this interval. At higher degrees of melting (~2% for fertile peridotite), however, where the compositions of fractional melts change more slowly than those of batch melts (per increment of melting), productivity for fractional melting is larger. Exhaustion of cpx from mantle source regions causes a sharp decrease in productivity owing to the change in reaction stoichiometry. This step change in productivity could play a role in localizing melt segregation in ascending mantle.

(4) Calculated isothermal addition of H_2O to hot peridotite shows that the amount of melting increases roughly linearly with the H_2O content of the system (rather than with the water content of the liquid), in agreement with the trend inferred by Stolper & Newman (1994) from examination of Mariana trough lavas. The extent of melting resulting from fluxing of peridotite with H_2O depends on whether the process is isothermal or isenthalpic. Because isenthalpic melting is accompanied by cooling, less melt is generated than if H_2O is added at constant temperature. Small quantities of H_2O greatly lower the solidus temperature of peridotite, but if the quantity of available water is limited, significant quantities of melt cannot form until temperatures at which large amounts of melt are generated under dry conditions; this is a consequence of the low productivities near the solidus of materials enriched in incompatible elements.

(5) The deepest melts generated during mantle upwelling are small proportions of melt formed in response to the solidus-lowering properties of CO_2, H_2O, and alkalis. There are likely to be several reasonably distinct deep, low-productivity zones in regions of upwelling, each dominated by a different flux (CO_2, H_2O, alkalis) and each affecting a different volume of mantle and producing melts of distinctive geochemical character. Analysis of any one of these sub-regimes without consideration of the effects of the others could lead to inaccurate models of behavior in this region. Very low melt productivities in these regions may greatly enhance development of U-series disequilibria.

ACKNOWLEDGEMENTS

We thank Bill Minarik, Glenn Gaetani, and Gautam Sen for thorough and constructive reviews. This work was supported by OCE-9711735 (M.M.H.), OCE-9529790 (M.S.G.) and EAR-9219899 and OCE-9504517 (E.M.S.). This paper is Caltech Division of Geological and Planetary Sciences Contribution 8510.

REFERENCES

Asimow, P. D. (1997). A thermodynamic model of adiabatic melting of the mantle. Ph.D. Thesis, Caltech, Pasadena, CA.

Asimow, P. D., Hirschmann, M. M., Ghiorso, M. S., O'Hara, M. J. & Stolper, E. M. (1995). The effect of pressure-induced solid–solid phase transitions on decompression melting of the mantle. *Geochimica et Cosmochimica Acta* **59,** 4489–4506.

Asimow, P. D., Hirschmann, M. M. & Stolper, E. M. (1997). An analysis of variations in isentropic melt productivity. *Philosophical Transactions of the Royal Society of London, Series A* **355,** 255–281.

Asimow, P. D., Hirschmann, M. M. & Stolper, E. M., 1999. Calculation of peridotite partial melting from thermodynamic models of minerals and melts. IV. Adiabatic decompression and the composition and mean properties of mid-ocean ridge basalts. *Journal of Petrology* (in preparation).

Baker, M. B. & Stolper, E. M. (1994). Determining the composition of high-pressure mantle melts using diamond aggregates. *Geochimica et Cosmochimica Acta* **58,** 2811–2827.

Baker, M. B., Hirschmann, M. M., Ghiorso, M. S. & Stolper, E. M. (1995). Compositions of near-solidus peridotite melts from experiments and thermodynamic calculations. *Nature* **375,** 308–311.

Beattie, P. (1993). Uranium–thorium disequilibria and partitioning on melting of garnet peridotite. *Nature* **363,** 63–65.

Blundy, J. D., Falloon, T. J., Wood, B. J. & Dalton, J. A. (1995). Sodium partitioning between clinopyroxene and silicate melts. *Journal of Geophysical Research* **100,** 15501–15515.

Blundy, J. D., Robinson, J. A. C. & Wood, B. J. (1998). Heavy REE are compatible in clinopyroxene on the spinel lherzolite solidus. *Earth and Planetary Science Letters* **160,** 493–504.

Bourdon, B., Zindler, A., Elliot, T. & Langmuir, C. H. (1996). Constraints on mantle melting at mid-ocean ridges from global ^{230}Th–^{238}U disequilibrium data. *Nature* **384,** 231–235.

Canil, D. & Scarfe, C. M. (1990). Phase relations in peridotite + CO_2 systems to 12 GPa: implications for the origin of kimberlite and carbonate stability in the Earth's upper mantle. *Journal of Geophysical Research* **95,** 15805–15816.

Carmichael, I. S. E., Turner, F. & Verhoogen, J. (1974). *Igneous Petrology*. New York: McGraw–Hill.

Davies, J. H. & Stevenson, D. J. (1992). Physical model of source regions of subduction zone volcanics. *Journal of Geophysical Research* **97,** 2037–2070.

Denbigh, K. (1981). *The Principles of Chemical Equilibrium*. Cambridge: Cambridge University Press.

Dick, H. J. B., Fischer, R. & Bryan, W. B. (1984). Mineralogic variability of the uppermost mantle along mid-ocean ridges. *Earth and Planetary Science Letters* **69,** 88–106.

Eggler, D. H. & Rosenhauer, M. (1978). Carbon dioxide in silicate melts. II. Solubilities of CO_2 and H_2O in $CaMgSi_2O_6$ (diopside) liquids and vapors at pressures to 40 kbars. *American Journal of Science* **278,** 64–94.

Gaetani, G. A. & Grove, T. L. (1998). The influence of water on mantle melting. *Contributions to Mineralogy and Petrology* **131,** 323–346.

Ghiorso, M. S. & Kelemen, P. (1987). Evaluating reaction stoichiometry in magmatic systems evolving under generalized thermodynamic constraints: examples comparing isothermal and isenthalpic assimilation. In: Mysen, B. O. (ed.) *Magmatic Processes: Physiochemical Principles. Geochemical Society Special Publication* **1,** 319–336.

Ghiorso, M. S. & Sack, R. O. (1995). Chemical mass-transfer in magmatic processes. 4. A revised and internally consistent thermodynamic model for the interpolation and extrapolation of liquid–solid equilibria in magmatic systems at elevated temperatures and pressures. *Contributions to Mineralogy and Petrology* **119,** 197–212.

Gill, J. (1981). *Orogenic Andesites and Plate Tectonics*. New York: Springer-Verlag.

Green, D. H. (1973). Experimental studies on a model upper mantle composition at high pressure under water-saturated and water-undersaturated conditions. *Earth and Planetary Science Letters* **19,** 37–53.

Herrstrom, E. A. (1998). Changes in histories of magmas and their sources along the Central American arc implied by uranium-series nuclide and trace element abundances. Ph.D. Thesis, University of Iowa, Iowa City.

Hirose, K. & Kawamoto, T. (1995). Hydrous partial melting of lherzolite at 1 GPa—the effect of H_2O on the genesis of basaltic magmas. *Earth and Planetary Science Letters* **133,** 463–473.

Hirose, K. & Kawamura, K. (1994). A new experimental approach for incremental batch melting of peridotite at 1·5 GPa. *Geophysical Research Letters* **21,** 2139–2142.

Hirose, K. & Kushiro, I. (1993). Partial melting of dry peridotites at high pressures: determination of compositions of melts segregated from peridotite using aggregates of diamond. *Earth and Planetary Science Letters* **114,** 477–489.

Hirschmann, M. M. & Stolper, E. M. (1996). A possible role for garnet pyroxenite in the origin of the 'garnet signature' in MORB. *Contributions to Mineralogy and Petrology* **124,** 185–208.

Hirschmann, M. M., Stolper, E. M. & Ghiorso, M. S. (1994). Perspectives on shallow mantle melting from thermodynamic calculations. *Mineralogical Magazine* **58A,** 418–419.

Hirschmann, M. M., Baker, M. B. & Stolper, E. M. (1998*a*). The effect of alkalis on the silica content of mantle-derived magmas. *Geochimica et Cosmochimica Acta* **62,** 883–902.

Hirschmann, M. M., Ghiorso, M. S., Asimow, P. D., Wasylenki, L. E. & Stolper, E. M. (1998*b*). Calculation of peridotite melting from thermodynamic models of minerals and melts. I. Methods and comparison to experiments. *Journal of Petrology* **39,** 1091–1115.

Hirschmann, M. M., Ghiorso, M. S. & Stolper, E. M. (1999). Calculation of peridotite partial melting from thermodynamic models of minerals and melts. II. Isobaric variations in melts near the solidus and owing to variable source composition. *Journal of Petrology* **40,** 297–313.

Hirth, G. H. & Kohlstedt, D. L. (1996). Water in the oceanic upper mantle: implications for rheology, melt extraction, and evolution of the lithosphere. *Earth and Planetary Science Letters* **144,** 93–108.

Iwamori, H. (1997*a*). Compression melting in subduction zones. *Terra Nova* **9,** 9–13.

Iwamori, H. (1997*b*). Heat sources and melting in subduction zones. *Journal of Geophysical Research* **102,** 14803–14820.

Iwamori, H., McKenzie, D. & Takahashi, E. (1995). Melt generation by isentropic mantle upwelling. *Earth and Planetary Science Letters* **134,** 253–266.

Jaques, A. L. & Green, D. H. (1980). Anhydrous melting of peridotite at 0–15 Kb pressure and the genesis of tholeiitic basalts. *Contributions to Mineralogy and Petrology* **73,** 287–310.

Kelemen, P. B., Shimizu, N. & Salters, V. (1995). Extraction of mid-ocean-ridge basalt from the upwelling mantle by focused flow of melt in dunite channels. *Nature* **375,** 747–753.

Kinzler, R. J. (1997). Melting of mantle peridotite at pressures approaching the spinel to garnet transition: application to mid-ocean ridge basalt petrogenesis. *Journal of Geophysical Research* **102,** 853–874.

Kinzler, R. J. & Grove, T. L. (1992). Primary magmas of mid-ocean ridge basalts. 2. Applications. *Journal of Geophysical Research* **97,** 6907–6926.

Klein, E. & Langmuir, C. H. (1987). Global correlations of ocean ridge basalt chemistry with axial depth and crustal thickness. *Journal of Geophysical Research* **92,** 8089–8115.

Kohlstedt, D. L., Keppler, H. & Rubie, D. C. (1996). Solubility of water in the alpha phase, beta phase and gamma phase of olivine. *Contributions to Mineralogy and Petrology* **123,** 345–357.

Kojitani, H. & Akaogi, M. (1997). Melting enthalpies of mantle peridotite: calorimetric determinations in the system CaO–MgO–Al_2O_3–SiO_2 and application to magma generation. *Earth and Planetary Science Letters* **153,** 209–222.

Kushiro, I. (1987). A petrological model of the mantle wedge and lower crust in the Japanese island arcs. In: Mysen, B. O. (ed.) *Magmatic Processes: Physiochemical Principles. Geochemical Society Special Publication* **1,** 165–181.

Langmuir, C. H., Klein, E. M. & Plank, T. (1992). Petrological systematics of mid-ocean ridge basalts: constraints on melt generation beneath ocean ridges. In: Morgan, J. P., Blackman, D. K. & Sinton, J. M. (eds) *Mantle Flow and Melt Generation at Mid-Ocean Ridges. Geophysical Monograph, American Geophysical Union* **71,** 183–280.

LaTourette, T. Z., Kennedy, A. K. & Wasserburg, G. J. (1993). Thorium–uranium fractionation by garnet: evidence for a deep source and rapid rise of oceanic basalts. *Science* **261,** 739–742.

Longhi, J. (1992). Origin of picritic green glass magmas by polybaric fractional fusion. *Proceedings of Lunar and Planetary Science* **22,** 343–353.

McCulloch, M. T. & Gamble, J. A. (1991). Geochemical and geodynamical constraints on subduction zone magmatism. *Earth and Planetary Science Letters* **102,** 358–374.

McKenzie, D. (1984). The generation and compaction of partial melts. *Journal of Petrology* **25,** 713–765.

McKenzie, D. (1985). ^{230}Th–^{238}U disequilibrium and the melting process beneath ridge axes. *Earth and Planetary Science Letters* **72,** 149–157.

McKenzie, D. & Bickle, M. J. (1988). The volume and composition of melt generated by extension of the lithosphere. *Journal of Petrology* **29,** 625–679.

McKenzie, D. & O'Nions, R. D. (1991). Partial melt distributions from inversion of rare earth element concentrations. *Journal of Petrology* **32,** 1021–1091.

Miller, G. H., Stolper, E. M. & Ahrens, T. H. (1991). The equation of state of a molten komatiite, 2, Applications to komatiite petrogenesis and the Hadean mantle. *Journal of Geophysical Research* **96,** 11849–11864.

Mysen, B. O. & Kushiro, I. (1977). Compositional variations of coexisting phases with degree of melting of peridotite in the upper mantle. *American Mineralogist* **62,** 843–865.

Niu, Y. L. & Batiza, R. (1991). An empirical method for calculating melt compositions produced beneath mid-ocean ridges: application to axis and off-axis (seamounts) melting. *Journal of Geophysical Research* **96,** 21753–21777.

Olafsson, M. & Eggler, D. H. (1983). Phase relations of amphibole, amphibole–carbonate, and phlogopite–carbonate peridotite: petrologic constraints on the asthenosphere. *Earth and Planetary Science Letters* **64,** 305–325.

Plank, T. & Langmuir, C. H. (1988). An evaluation of the global variations in the major element chemistry of arc basalts. *Earth and Planetary Science Letters* **90,** 349–370.

Plank, T. & Langmuir, C. H. (1992). Effects of the melting regime on the composition of the oceanic crust. *Journal of Geophysical Research* **97,** 19749–19770.

Plank, T., Spiegelman, M., Langmuir, C. H. & Forsyth, D. W. (1995). The meaning of F—clarifying the mean extent of melting at ocean ridges. *Journal of Geophysical Research* **100,** 15045–15052.

Presnall, D. C. (1969). The geometrical analysis of partial fusion. *American Journal of Science* **267,** 1178–1194.

Robinson, J. A. C., Wood, B. J. & Blundy, J. D. (1998). The beginning of melting of fertile and depleted peridotite at 1·5 GPa. *Earth and Planetary Science Letters* **155,** 97–111.

Scott, D. R. (1992). Small-scale convection and mantle melting beneath mid-ocean ridges. In: Morgan, J. P., Blackman, D. K. & Sinton, J. M. (eds) *Mantle Flow and Melt Generation at Mid-Ocean Ridges. Geophysical Monograph, American Geophysical Union* **71,** 327–352.

Shaw, D. M. (1970). Trace element fractionation during anatexis. *Geochimica et Cosmochimica Acta* **34,** 237–243.

Sisson, T. W. & Bronto, S. (1998). Evidence for pressure-release melting beneath magmatic arcs from basalt at Galunggung, Indonesia. *Nature* **391,** 883–886.

Sleep, N. H. (1984). Tapping of magmas from ubiquitous mantle heterogeneities; an alternative to mantle plumes? *Journal of Geophysical Research* **89,** 29–41.

Spiegelman, M. (1993). Flow in deformable porous-media 1. Simple analysis. *Journal of Fluid Mechanics* **247,** 17–38.

Spiegelman, M. & Elliott, T. (1993). Consequences of melt transport for uranium series disequilibrium in young lavas. *Earth and Planetary Science Letters* **118,** 1–20.

Stolper, E. M. & Newman, S. (1994). The role of water in the petrogenesis of Mariana Trough magmas. *Earth and Planetary Science Letters* **121,** 293–325.

Takahashi, E., Shimazaki, T., Tsuzaki, Y. & Yoshida, H. (1993). Melting study of a peridotite KLB-1 to 6·5 GPa, and the origin of basaltic magmas. *Philosophical Transactions of the Royal Society of London, Series A* **342,** 105–120.

Tatsumi, Y. (1983). Generation of arc basalt magmas and thermal structure of the mantle wedge in subduction zones. *Journal of Geophysical Research* **88,** 5815–5825.

Tatsumi, Y., Hamilton, D. L. & Nesbitt, R. W. (1986). Chemical characteristics of fluid phase released from a subducted lithosphere and origin of arc magmas: evidence from high-pressure experiments and natural rocks. *Journal of Volcanology and Geothermal Research* **29,** 293–309.

Walter, M. J. & Presnall, D. C. (1994). Melting behavior of simplified lherzolite in the system CaO–MgO–Al_2O_3–SiO_2–Na_2O from 7 to 35 kbar. *Journal of Petrology* **35,** 329–359.

Wasylenki, L. E., Baker, M. B., Hirschmann, M. M. & Stolper, E. M. (1996). The effect of source depletion on equilibrium mantle melting. *EOS Transactions, American Geophysical Union* **77,** 847.

Williams, R. W. & Gill, J. B. (1989). Effects of partial melting on the uranium decay series. *Geochimica et Cosmochimica Acta* **53,** 1607–1619.

Wyllie, P. J. (1979). Magmas and volatile components. *American Mineralogist,* **64,** 469–500.